

Ph.D. Course in Mathematical Models for Engineering,
Electromagnetism and Nanosciences
Open Day, November 21, 2018

Electromagnetism Curriculum

Fabrizio Frezza

Electromagnetic Fields 2 Lab website: <http://labcem2.diet.uniroma1.it>

Prof. Fabrizio Frezza website: <http://labcem2.diet.uniroma1.it/fabriziofrezza>



Curriculum Professors (XXXIV Cicle)

Eugenio Fazio

Fabrizio Frezza

Marco Rossi

Adalberto Sciubba

Concita Sibilia

Giuseppe Zollo

Offered Courses

Corso di scrittura tecnico-scientifica (3 CFU), prof. Emilio Matricciani (Polytechnic of Milan), 29 and 30 January, 5 and 6 February 2019 (room 7, via Eudossiana)

E1. Artificial Materials, Metamaterials and Plasmonics for electromagnetic applications (3 CFU) - II sem., prof. Fabrizio Frezza (Sapienza University of Rome)

Program: Frequency Selective Surfaces (FSS) and applications. Photonic (PBG) or Electromagnetic (EBG) Crystals and applications. Metamaterials and applications. The wire medium. Surface Plasmons and applications.

E2. Nanophotonics and Plasmonics (2 CFU) - II sem. prof. Concita Sibilìa (Sapienza University of Rome)

Program: The part of seminars related to Nanophotonics aims to introduce to students some exciting concepts that differ from conventional wave optics, with particular emphasis to the role of the evanescent fields in many practical applications, such as near field optical microscopy. The field of plasmonics (interaction of light with electrons in metals) has attracted a great deal of interest over the past two decades, but despite the many fundamental breakthroughs and exciting science it has produced, it is yet to deliver on the applications that were initially targeted as most promising. The seminars proposed examine the primary fundamental hurdles in the physics of plasmons that have been hampering practical applications and highlights some of the promising areas in which the field of plasmonics can realistically deliver.

E3. Basics of Nonlinear Optics (2 CFU) - II sem. prof. Concita Sibilìa (Sapienza University of Rome)

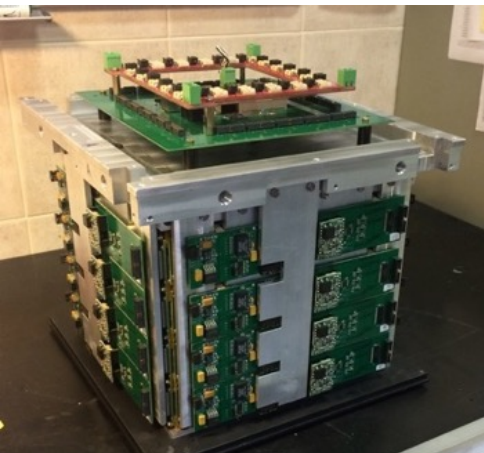
Program: Nonlinear Optics (NLO) is the study of phenomena that occur as a consequence of the modification of the optical properties of a material system by the presence of light. Basics and more recent applications of NLO to new light sources and devices will be presented in a series of seminars.

From the curriculum Mathematics for Engineering: Partial differential equations and applications Daniele Andreucci, 12 hours (M3)

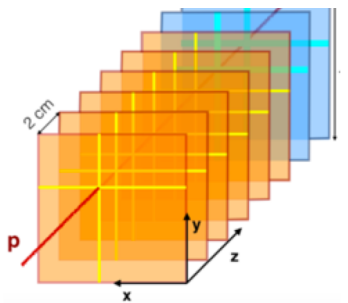
List of useful Courses from the Master degree:

- **Master E1:** Advanced Electromagnetics and Scattering (6 CFU), II sem., prof. Fabrizio Frezza (Sapienza University of Rome)
- **Master E2:** Nanostructured materials and components for electromagnetic applications (6 CFU), II sem., prof. Fabrizio Frezza (Sapienza University of Rome)
- **Master E3:** Laser fundamentals (6 CFU), II sem., prof. Concita Sibilìa (Sapienza University of Rome)
- **Master E4:** Tecnologie di fabbricazione di nanostrutture e processi di autoassemblaggio (6 CFU), II sem., prof. Carlo Mariani (Sapienza University of Rome)
- **Master E5:** Microscopie e tecniche di nanocaratterizzazione (9 CFU), II sem., prof. Marco Rossi (Sapienza University of Rome)
- **Master E6:** Modelli e tecniche di simulazione atomistica (6 CFU), II sem., prof. Giuseppe Zollo (Sapienza University of Rome)

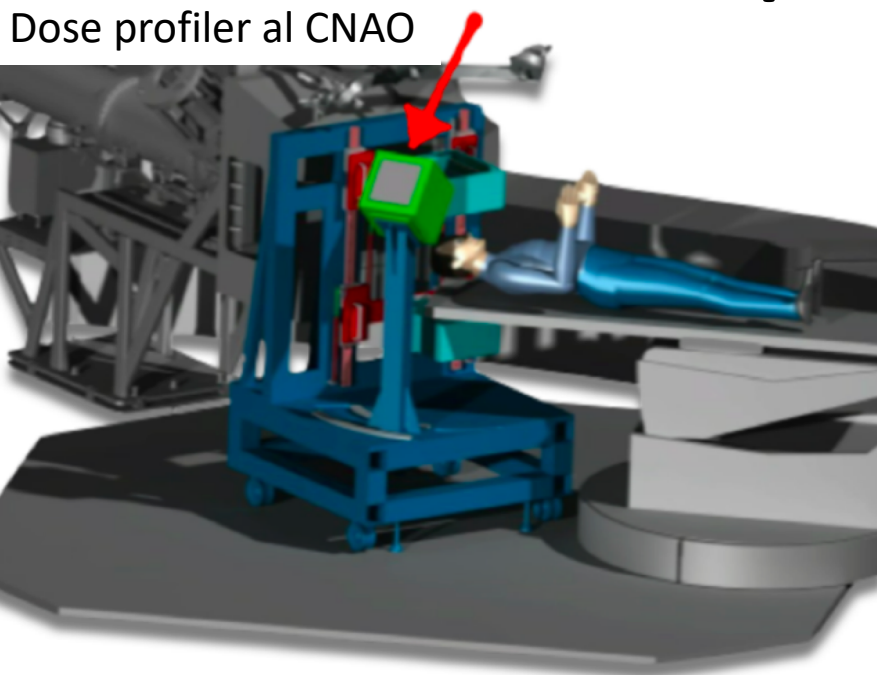
Ricerca & Sviluppo delle tecnologie fisiche in radioterapia



Dose profiler
(3000 silicon photomultiplier)

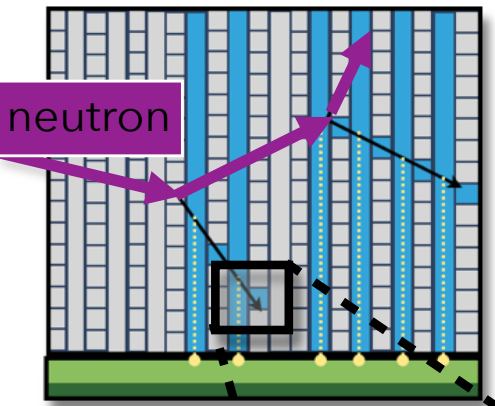


Prototipi di monitor di dose da radiazione e loro impiego in trial clinici



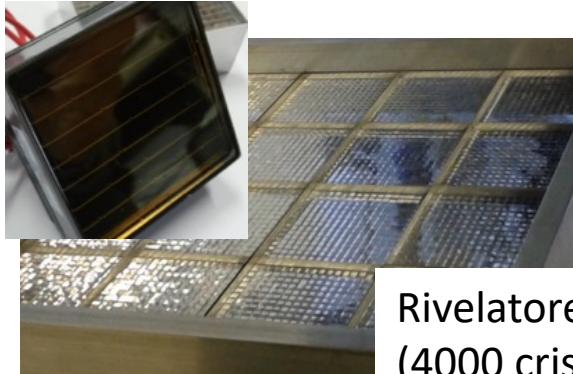
Dose profiler al CNAO

Rivelatore MONDO
10 x10x20 cm³
30 km fibre scintillanti



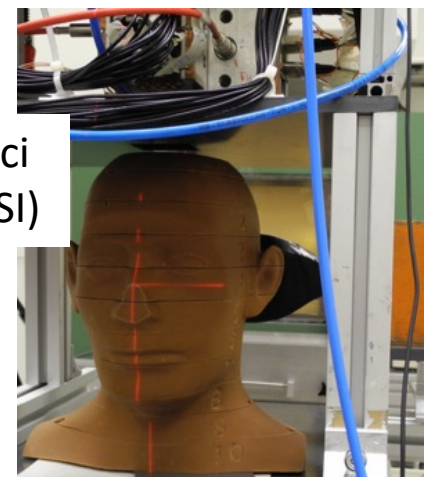
neutron

photon



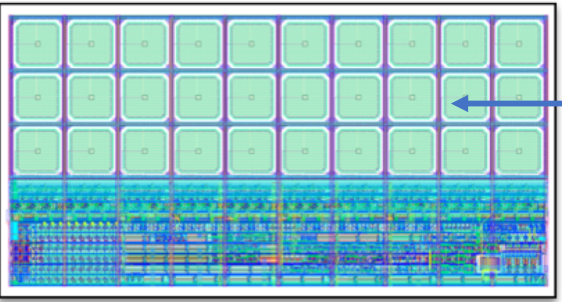
Rivelatore PET
(4000 cristalli)

Misure su fantocci antropomorfi (GSI)

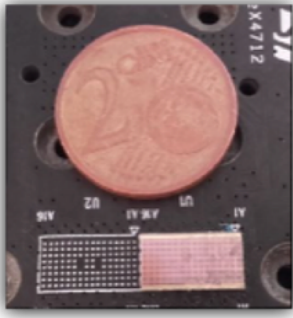


Ricerca & Sviluppo delle tecnologie fisiche in radioterapia

Sviluppo di microelettronica per sensori innovativi



125 x 250 μm pixel
misura di carica e tempi



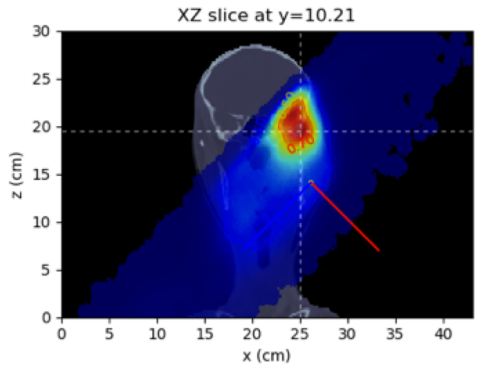
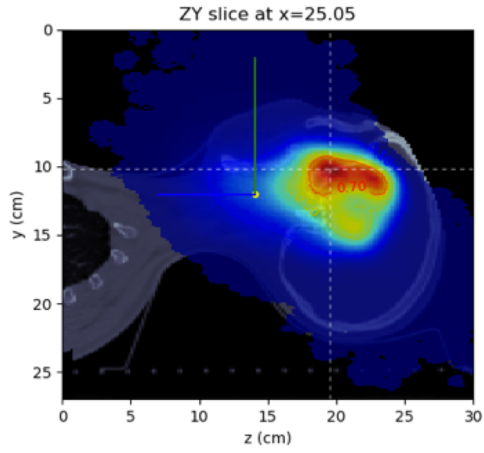
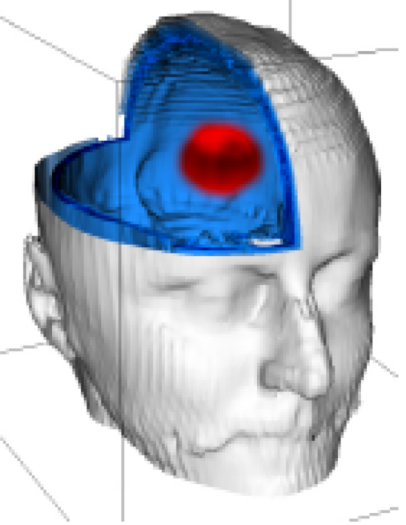
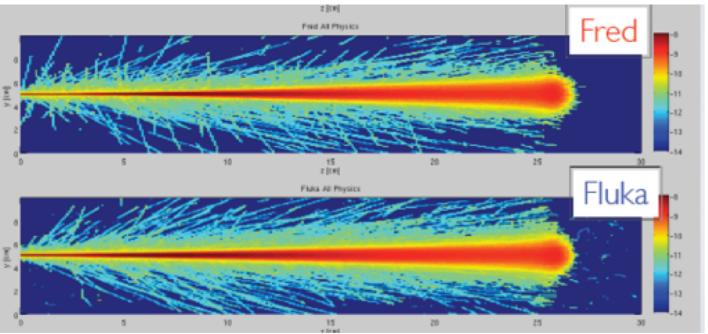
3000 pixel/cm²

Software per ricostruzione di immagini

in presenza di assorbimento nella materia

Tecniche di fast Montecarlo su GPU

→ certificazione di piani terapeutici





SAPIENZA
UNIVERSITÀ DI ROMA

Concita Sibilìa

A. Belardini, G. Leahu, E. Ptronijevic,
M.Centini, R.Li Voti,G. M. Cesarini, L.Gallottini,M.C.Larciprete

*Dipartimento di Scienze di Base e Applicate per l'Ingegneria
Sapienza Università di Roma
Roma, Italy*

Attività di Ricerca

Optics, Nonlinear Optics,
Materials, Metamaterials,
Optothermal properties of
materials- Theory and
Experiments

Attività didattica

Laser Physics
Nonlinear Optics
Plasmonics

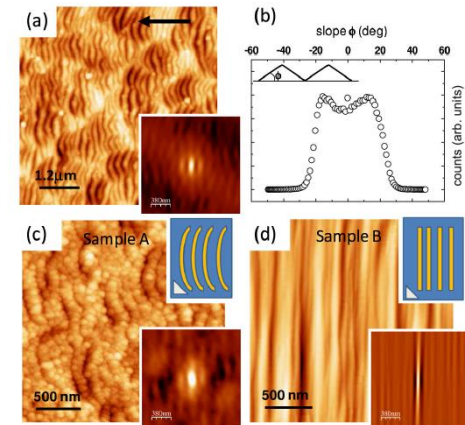
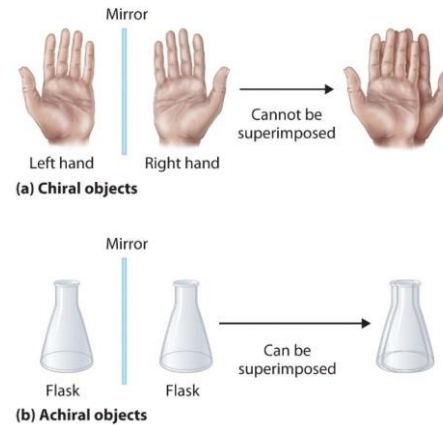
II Level Master In Optics and
Quantum Information
www.sbai.uniroma1.it ,
www.masteroqi.uniroma1.it

Materiali Otticamente chirali- Metamateriali ottici Ottica Nonlineare-SHG

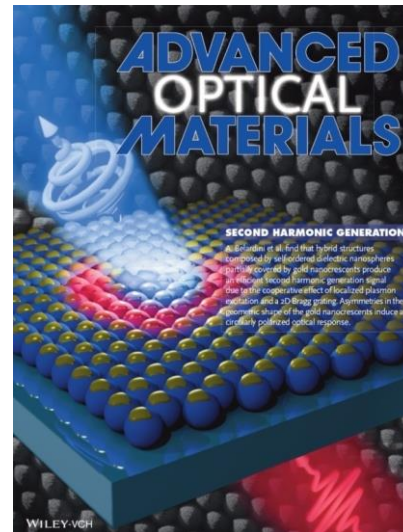
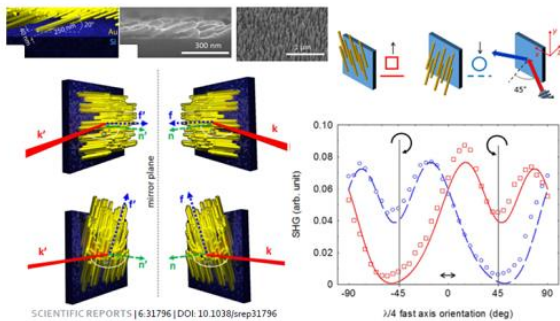
Circular Dichroism in the Optical Second-Harmonic Emission of Curved Gold Metal Nanowires

A. Belardini,^{*} M. C. Larciprete, M. Centini, E. Fazio, and C. Sibilia
Dipartimento di Scienze di Base e Applicate per l'Ingegneria, Sapienza Università di Roma and CNISM,
Via A. Scarpa 16, I-00161 Roma, Italy

D. Chiappe, C. Martella, A. Toma,[†] M. Giordano, and F. Buatier de Mongeot
Istituto di Fisica, Università di Genova and CNISM, Via Dodecaneso 33, 16146 Genova, Italy
(Received 8 June 2011; published 12 December 2011)



SCIENTIFIC REPORTS | 6:31796 | DOI: 10.1038/srep31796
SCIENTIFIC REPORTS



A. Belardini et al.,
Adv. Opt. Mat., 2, 208-213
(2014).

Sorgenti Laser dal vicino UV al THz

Teoria ed esperimenti

- Interazione ottica lineare e nonlineare anche alla nanoscala
- Schemi di laser -cristalli fotonici
- Cristalli plasmonici

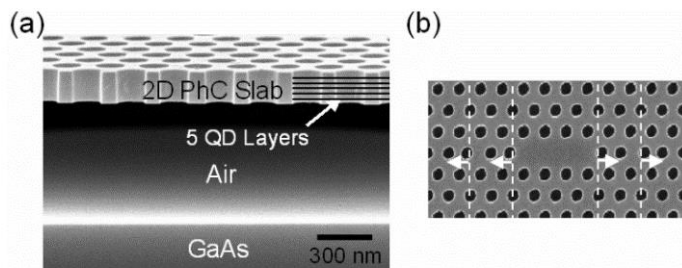
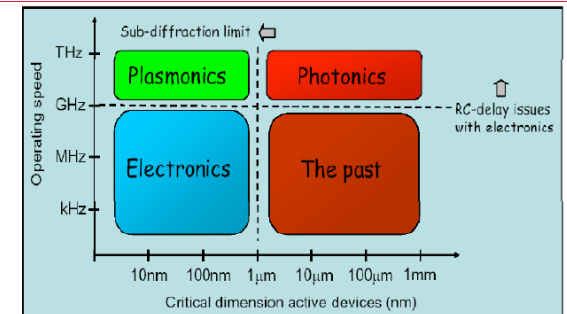
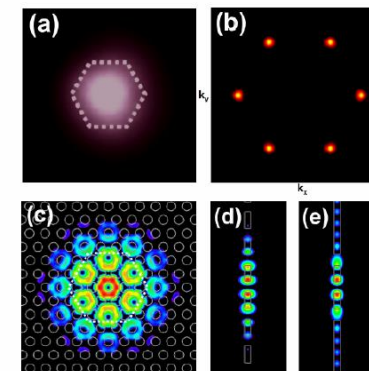
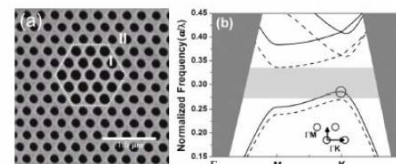


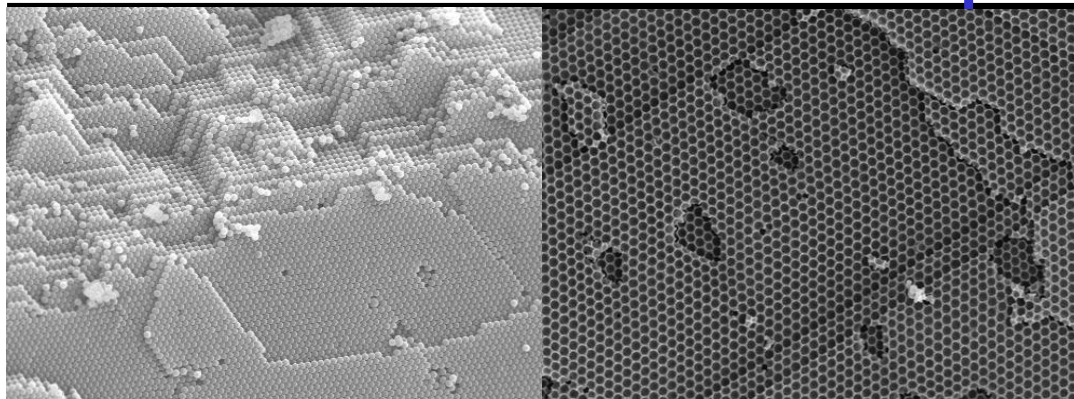
Fig. 1. (a) Scanning electron micrograph of a cross section of a two-dimensional PhC structure. (b) Top view of the L3 defect nanocavity. The first and third nearest air holes at both ends of the cavity are shifted outwards by $0.15a$ as shown by white arrows.



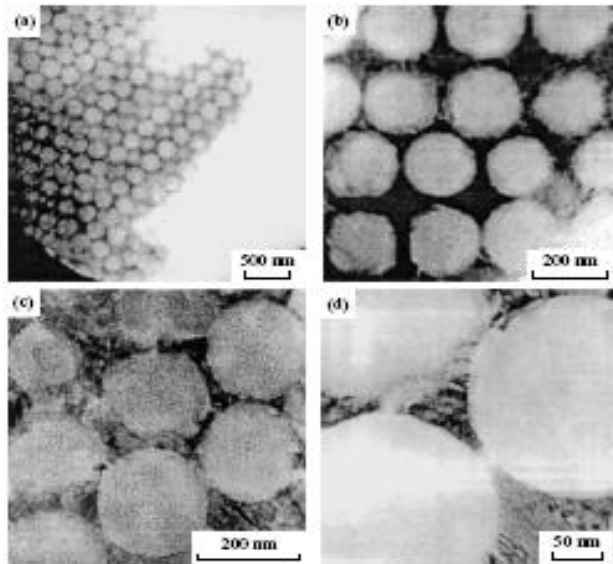
- Quantum information: sorgenti a singolo fotone, sorgenti nonlineari (oscillatori parametrici)

Optothermal properties at nanoscale

Struttura opale

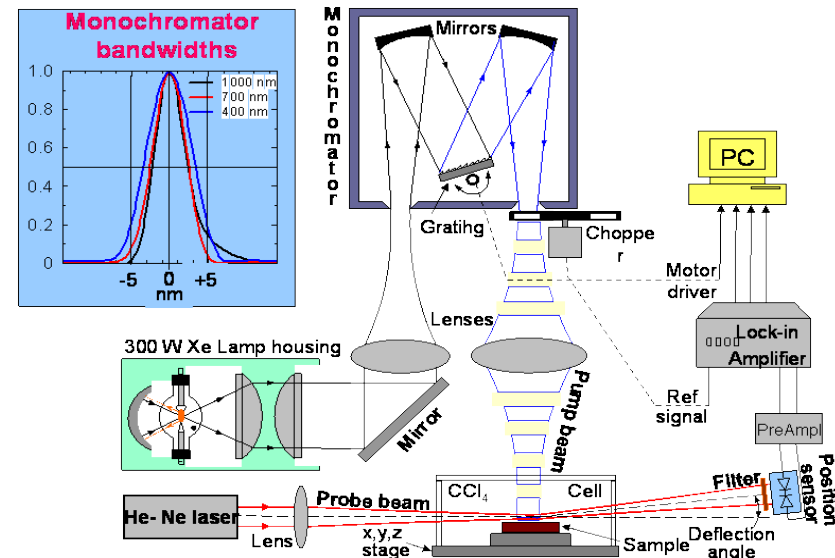
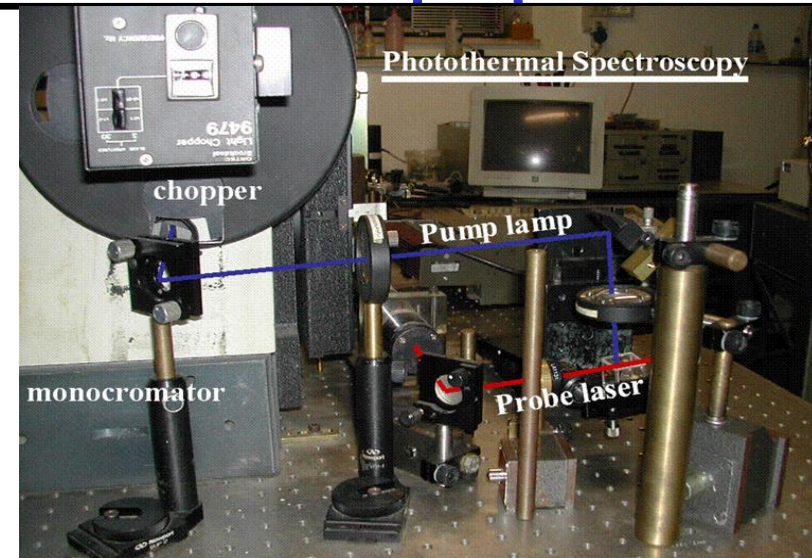


Struttura opale diretta ed inversa - C.Lopez - CSIC Madrid



Opali Silica-GaN - V.Golubev - JOFFE - S.Petersburg

Set-up Sperimentale



Modeling -Nanoplasmonics

- Propagazione di impulsi elettromagnetici in materiali metallo-dielettrico non omogenei con non linearità del secondo e terzo ordine
- Nanoantenne anche nel vicino IR

Metodi numerici e analitici:

1- FFT Beam propagation method modificato: simulazione di impulsi corti attraverso strutture non omogenee dielettriche e metallo dielettriche.

2- FDTD: software commerciale Optiwave e Lumerical, per design e simulazione di strutture a guide d'onda, cristalli fotonici bidimensionali, materiali ad indice di rifrazione negativo.

3- Elementi finiti: Comsol multiphysics con pacchetto elettromagnetico.

Relazioni con il mondo del lavoro

Ricerca fondamentale, ricerca applicata e industriale ad alta tecnologia con uso di laser ed ottica :

- Collaborazioni con università ed istituti di ricerca italiani e stranieri.
- SBAI fa parte di EPIC, consorzio europeo nelle tecnologie ottiche.
- Interazione con grossi gruppi industriali dell'area laziale (Leonardo, Elettronica, Thales)



COST MP1403- Nanoscale Quantum Optics

UE project-
ENSEMBLE3- Center
of Excellence in
Nanophotonics

Recent progress in the research of Electromagnetic-wave propagation and scattering

Fabrizio Frezza (via Eudossiana 18, DIET, room no. 317, 3rd floor)



Department of Information Engineering, Electronics and Telecommunications (DIET)

Advanced Electromagnetics and Scattering
(M.Sc. Electronics Engineering and M.Sc. Atmospheric Science and Technology)

Artificial Materials, Metamaterials and Plasmonics for Electromagnetic Applications
(M.Sc. Nanotechnology Engineering)

Basic Electromagnetic Fields (in Italian, B.Sc. Information Engineering, Latina)

Laboratory of Electromagnetic Fields 2 (LabCEM2)

fabrizio.frezza@uniroma1.it

Skype: fabriziofrezza

<http://labcem2.diet.uniroma1.it/fabriziofrezza>

https://www.researchgate.net/profile/Fabrizio_Frezza

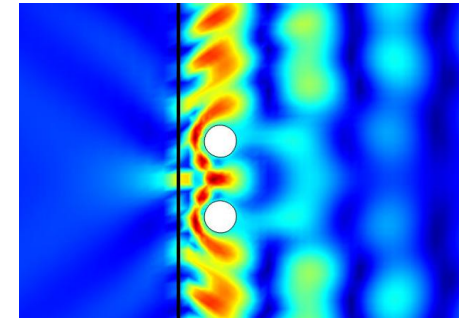
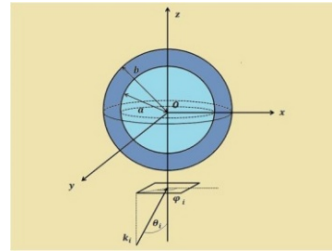


Outline

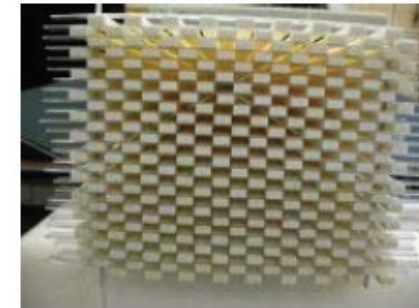
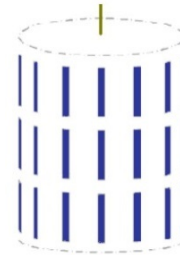
- Electromagnetic scattering from buried objects
- Electro-Thermal Passive Intermodulation due to Conductor Surface Roughness
- Ground Penetrating Radar (GPR), COST Action TU1208
- Biomedical space applications
- Metamaterials
- Frequency-selective surfaces (FSSs) for field absorbers
- Leaky-Wave Antennas
- Electromagnetic-wave propagation in lossy media
- European School of Antennas (ESoA): 5th Edition of the Course, April 2017
- Magnetic Resonance Imaging (MRI)
- Sensor Networks, Remote Sensing
- Cultural Heritage

Research topics

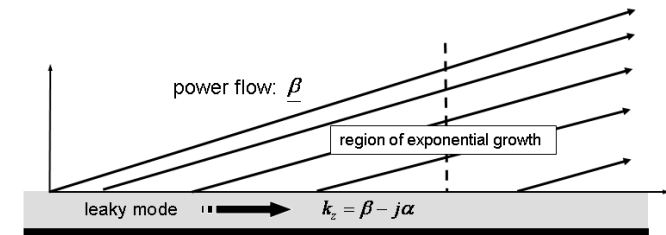
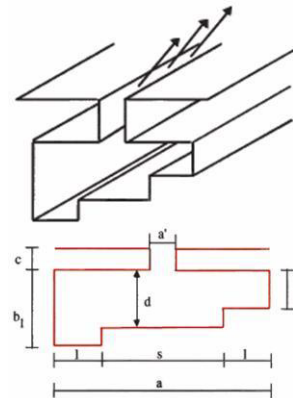
Scattering by 2D/3D buried objects in lossy media



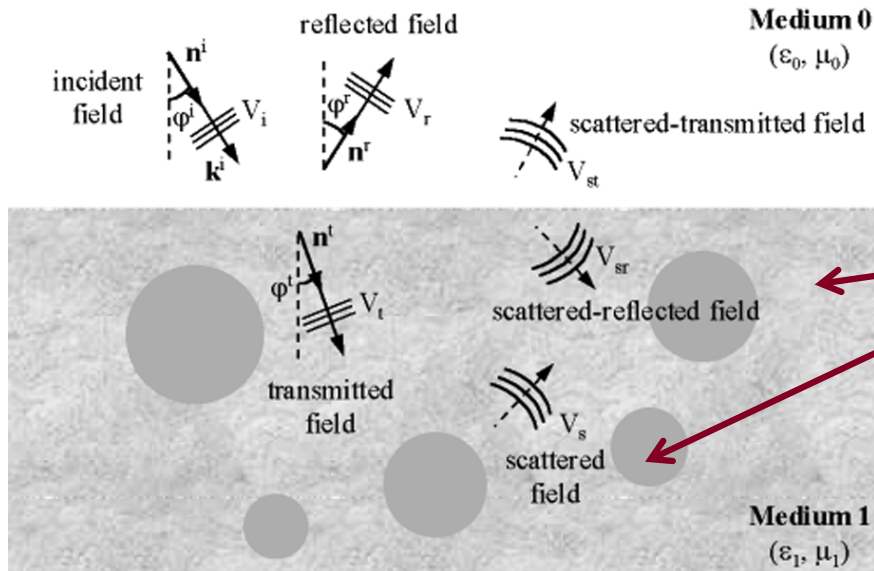
Metamaterials



Leaky-Wave Antennas



Scattering by Buried Objects Cylindrical Structures (1)



The representation of these fields requires the plane-wave spectrum of cylindrical functions.

N cylinders \longleftrightarrow N reference systems

Dissipative media

Wave Decomposition:

- Incident
- Reflected
- Transmitted

$$e^{i\vec{k}\cdot\vec{r}} = \sum_{m=-\infty}^{+\infty} J_n(\rho_n) e^{im\theta_n}$$

- Scattered $\longrightarrow \sum_{m=-\infty}^{+\infty} c_{mn} H_m^{(1)}(\rho_n) e^{im\theta_n}$

? {

- Scattered-Reflected
- Scattered-Transmitted

Scattering by Buried Objects

Cylindrical Structures (2)

Interaction between cylindrical waves and the plane interface:

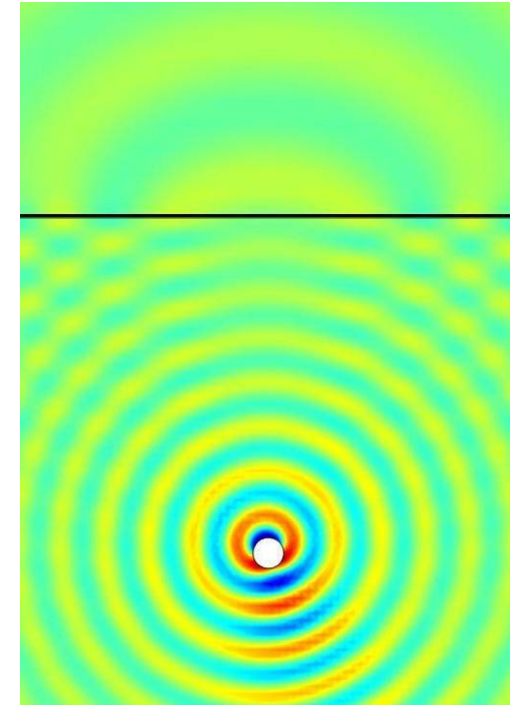
$$H_m^{(1)}(\rho_n) e^{im\theta_n} = \int_{-\infty}^{+\infty} F_m(\xi_n, n_{\parallel}) e^{in_{\parallel}\zeta_n} dn_{\parallel}$$

Plane-Wave Spectrum of Cylindrical Functions

Multiplying by the Fresnel Coefficients:

$$RW_m(\xi_n, \zeta_n) = \int_{-\infty}^{+\infty} \Gamma(n_{\parallel}) F_m(\xi_n, n_{\parallel}) e^{in_{\parallel}\zeta_n} dn_{\parallel}$$

$$TW_m(\xi_n, \zeta_n) = \int_{-\infty}^{+\infty} T(n_{\parallel}) F_m(\xi_n, n_{\parallel}) e^{i(\xi_n + \chi_n)\sqrt{1-n_{\parallel}^2}} e^{in_{\parallel}\zeta_n} dn_{\parallel}$$



All quantities are in the reference system of each cylinder!!!

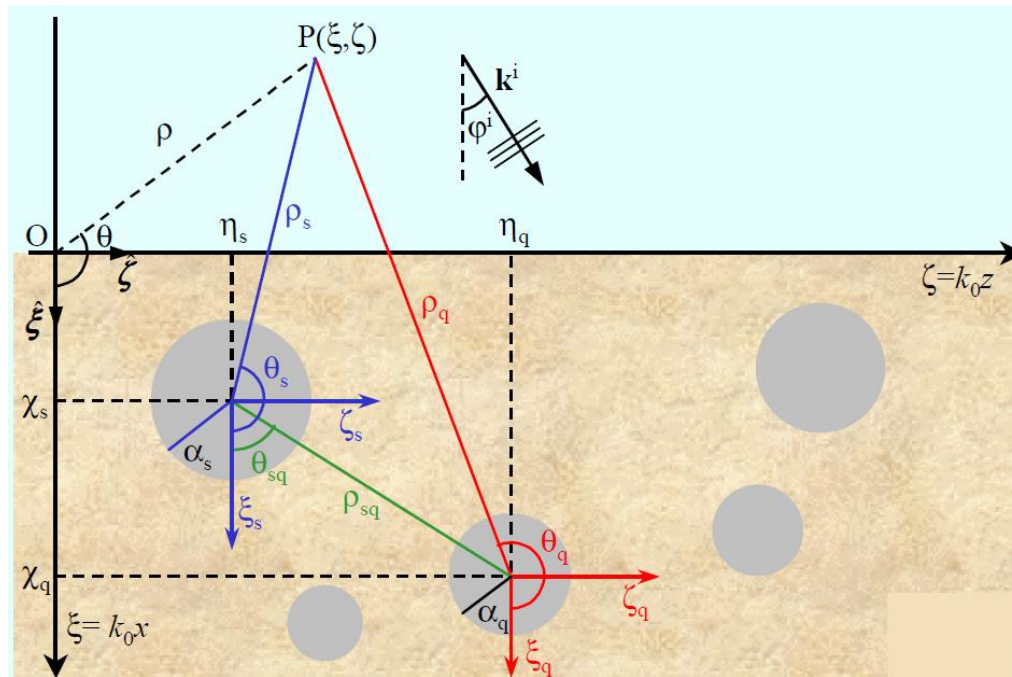
Scattering by Buried Objects

Cylindrical Structures (3)

To impose the boundary conditions on the surface of each s-th cylinder the scattered field by each q-th cylinder must be expressed in the s-th reference frame:

Graf Addition Formula

$$H_m^{(1)}(\rho_q) e^{im\theta_q} = e^{im\theta_{sq}} \sum_{n=-\infty}^{+\infty} (-1)^n H_{m+n}^{(1)}(\rho_{sq}) e^{in\theta_{sq}} J_n(\rho_s) e^{in\theta_s}$$



The boundary conditions give:

$$\sum_{n=1}^N \sum_{p=-\infty}^{+\infty} A_{np}^{ms} c_{np} = B_{ms} \quad \begin{array}{l} m = 0, \pm 1 \dots \\ s = 1, 2 \dots N \end{array}$$

Where A_{np}^{ms} and B_{ms} are known.

c_{np} Are the unknown and can be found by a suitable truncation.

A (not so simple) Fortran code has been implemented for their calculation!

Scattering by Buried Objects

Spherical Structures (1)

The shape is different, the procedure is the same.

Incident and scattered fields can be represented with the **spherical-wave vector functions**:

$$E_i = \sum_{q=1}^{\infty} \sum_{p=-q}^q \left[a_{pq} \vec{M}_{pq}^{(1)}(\vec{r}) + b_{pq} \vec{N}_{pq}^{(1)}(\vec{r}) \right]$$

$$E_s = \sum_{q=1}^{\infty} \sum_{p=-q}^q \left[c_{pq} \vec{M}_{pq}^{(3)}(\vec{r}) + d_{pq} \vec{N}_{pq}^{(3)}(\vec{r}) \right]$$

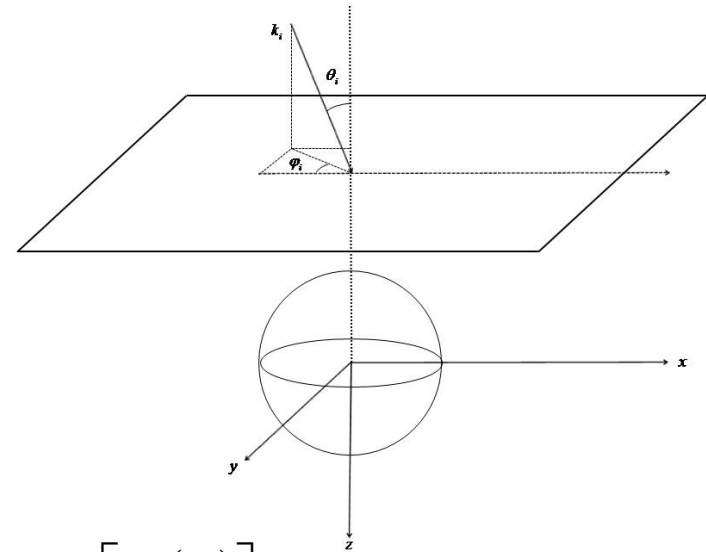
$$M_{pq}^{(1)}(\vec{r}) = j_q(\rho) \vec{m}_{pq}(\theta, \varphi) \quad N_{pq}^{(1)}(\vec{r}) = \frac{j_q(\rho)}{\rho} \vec{p}_{pq}(\theta, \varphi) + \frac{1}{\rho} \frac{\partial [j_q(\rho)]}{\partial \rho} \vec{n}_{pq}(\theta, \varphi)$$

$$M_{pq}^{(3)}(\vec{r}) = h_q^{(1)}(\rho) \vec{m}_{pq}(\theta, \varphi) \quad N_{pq}^{(3)}(\vec{r}) = \frac{h_q^{(1)}(\rho)}{\rho} \vec{p}_{pq}(\theta, \varphi) + \frac{1}{\rho} \frac{\partial [h_q^{(1)}(\rho)]}{\partial \rho} \vec{n}_{pq}(\theta, \varphi)$$

$\vec{m}_{pq}(\theta, \varphi)$, $\vec{n}_{pq}(\theta, \varphi)$, $\vec{p}_{pq}(\theta, \varphi)$ are the **Tesseral Vector Functions**.

They are orthogonal to one another!!

They are strongly connected with the Tesseral Scalar Function: $Y_{pq}(\theta, \varphi) = P_q^p(\cos \theta) e^{ip\varphi}$



Scattering by Buried Objects

Spherical Structures (2)

This time, we need the plane-wave spectrum of spherical functions.

$$j_q(k\rho)Y_{pq}(\theta, \varphi) = \frac{i^{-n}}{4\pi} \int_0^{2\pi} \int_0^\pi Y_{pq}(\alpha, \beta) \sin \alpha e^{i\vec{k}\cdot\vec{r}} d\alpha d\beta$$

Scalar spherical functions
(Whittaker, 1902)
(Erdélyi, 1937)

$$h_q^{(1)}(k\rho)Y_{pq}(\theta, \varphi) = \frac{i^{-n}}{4\pi} \int_0^{2\pi} \int_0^{\pi/2-i\infty} Y_{pq}(\alpha, \beta) \sin \alpha e^{i\vec{k}\cdot\vec{r}} d\alpha d\beta$$

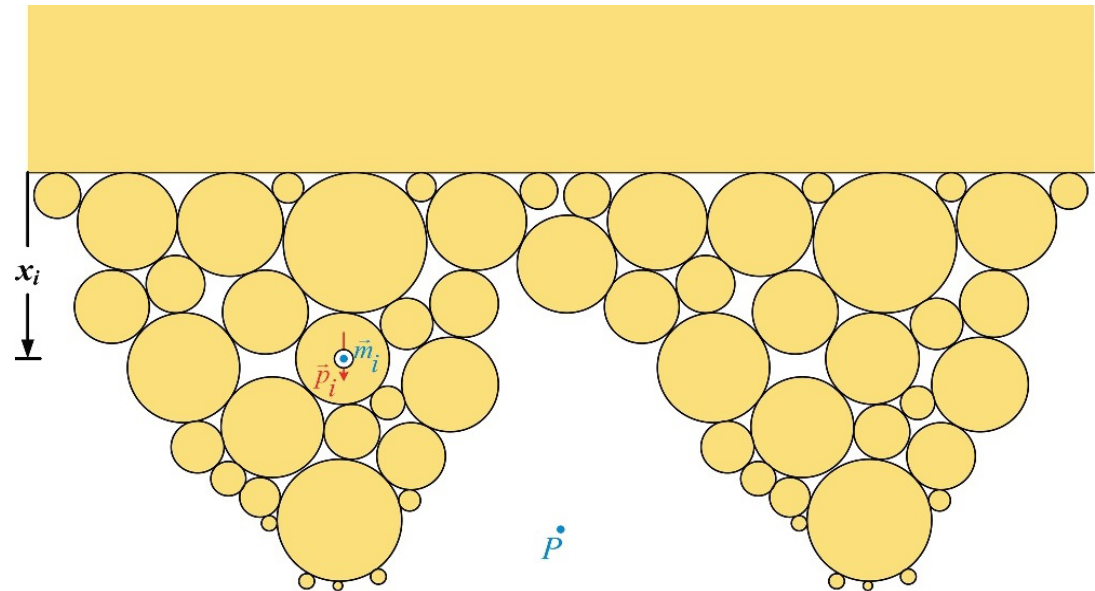
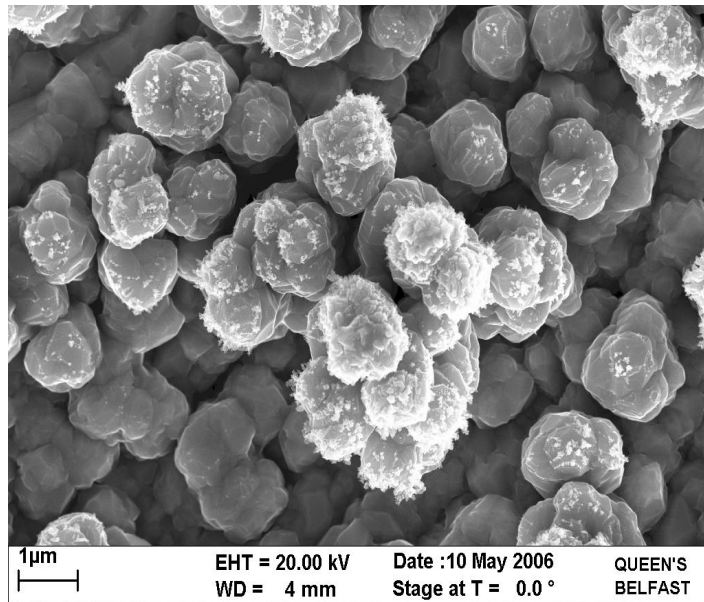
By a few calculations:

$$\vec{M}_{pq}^{(3)}(\theta, \varphi) = \frac{i^{-n}}{2\pi} \int_0^{2\pi} \int_0^{\pi/2-i\infty} \vec{m}_{pq}^{(3)}(\alpha, \beta) \sin \alpha e^{i\vec{k}\cdot\vec{r}} d\alpha d\beta$$

$$\vec{N}_{pq}^{(3)}(\theta, \varphi) = \frac{i^{-n}}{2\pi} \int_0^{2\pi} \int_0^{\pi/2-i\infty} \vec{n}_{pq}^{(3)}(\alpha, \beta) \sin \alpha e^{i\vec{k}\cdot\vec{r}} d\alpha d\beta$$

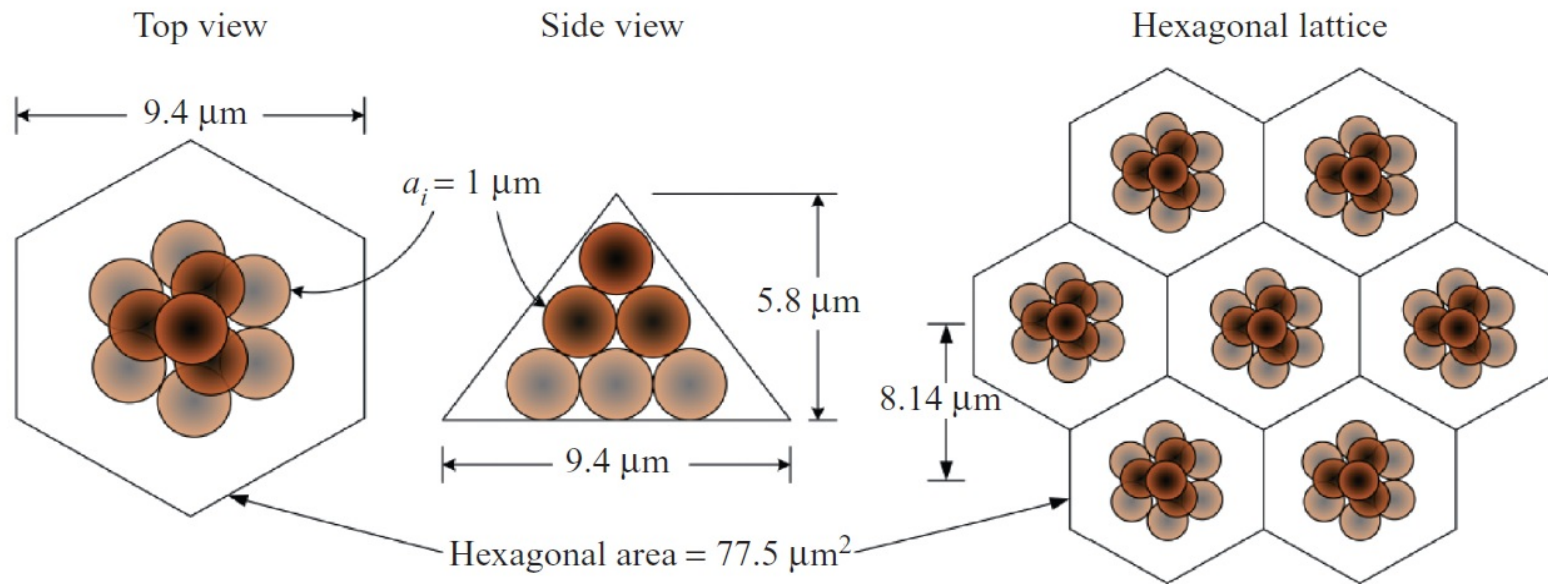
Exploiting the orthogonality of the tesseral vector functions and imposing the boundary conditions, a linear system for the coefficients can be found.

Electro-Thermal Passive Intermodulation due to Conductor Surface Roughness (Dr. A. Schuchinsky, Dr. A. Shitvov)



Small imperfect conductor balls are clustered to model dendrites of copper foils

Surface Roughness model



When a small copper sphere of radius a_i is exposed to an external electric and magnetic field it acts as an electric and magnetic dipoles. The propagating wave scattering and absorption by the dipoles can be calculated.

COST Action TU1208

Civil Engineering Applications of Ground Penetrating Radar



<http://gpradar.eu>



Working Group 1

- Design of innovative GPR equipment dedicated for CE applications
- Prototypes design
- Testing and optimization of the new system.

Working Group 2

- Surveying, through the use of a GPR system, of pavement, bridges, tunnels and buildings.
- Sensing of underground utilities and voids.

Working Group 3

- EM-scattering methods for the characterization of scenarios that are of interest in GPR and CE fields
- Effective data-processing algorithms for the elaboration of GPR data collected during CE surveys.

Working Group 4

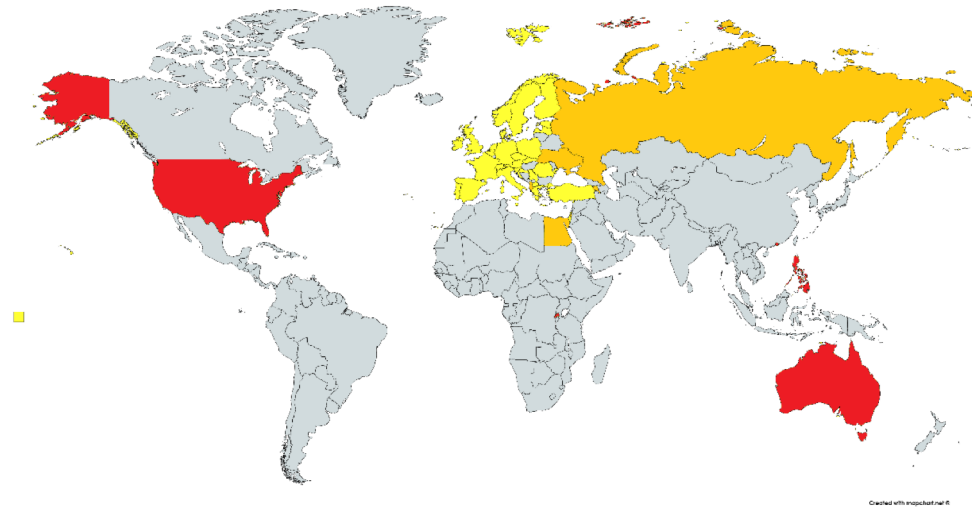
- Different applications of GPR and on other NDT techniques for CE.

COST Action TU1208

Civil Engineering Applications of Ground Penetrating Radar

Represented Nations

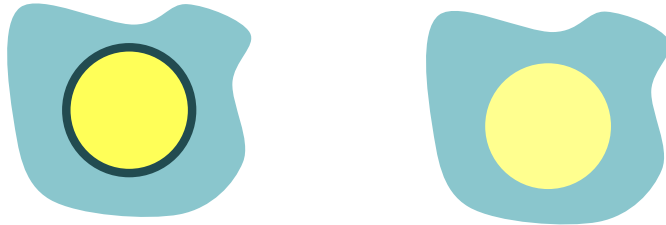
- Austria
- Belgium
- Croatia
- Czech Republic
- Denmark
- Estonia
- Finland
- France
- fYR Macedonia
- Germany
- Greece
- Ireland
- Italy
- Latvia
- Malta
- Netherlands
- Norway
- Poland
- Portugal
- Romania
- Serbia
- Slovakia
- Slovenia
- Spain
- Sweden
- Switzerland
- Turkey
- United Kingdom
- Israel
- Albania
- Armenia
- Egypt
- Palestine
- Russia
- Ukraine
- Australia
- Hong Kong
- Philippines
- Rwanda
- USA



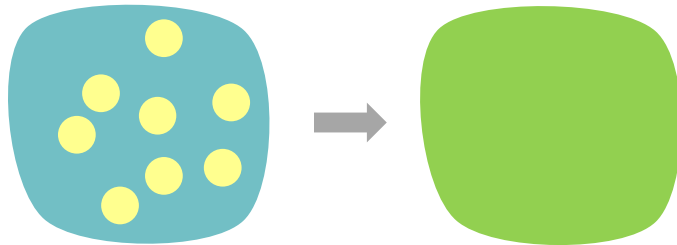
CellTer – Italian Space Agency (ASI) research project

3D evaluation techniques of cellular growth and morphology in microgravity conditions through electromagnetic diffraction

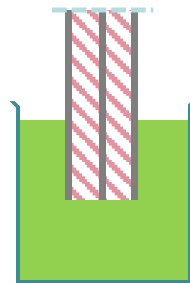
1 Particles homogenization



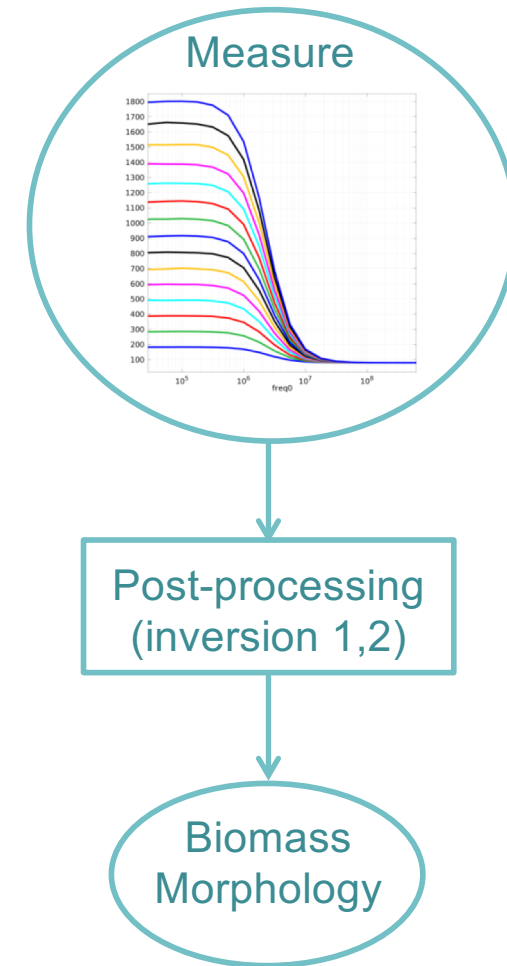
2 Mixture homogenization



3 Measurement of permittivity with a coaxial probe



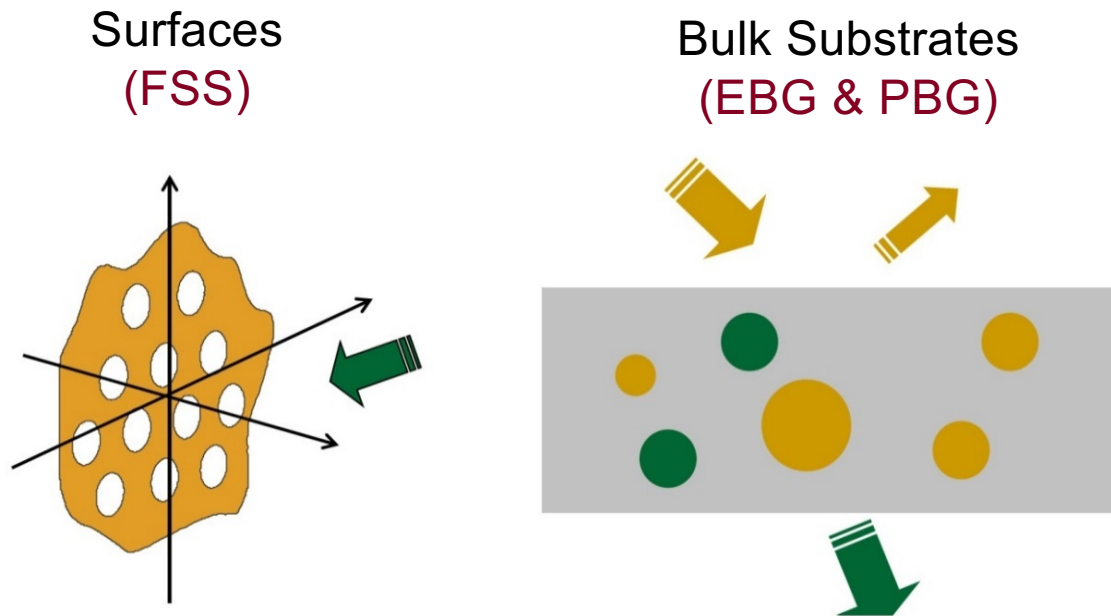
4 Estimation of the biomass and morphology



Metamaterials

Structures that possess a **spatial periodicity**.

They can be 2D or 3D structures, with 1D, 2D, or 3D periodicity.



Analysis techniques:

- Method of Moments with the Floquet analysis
- Finite-Difference Time-Domain Method

Metamaterials

FSS (1)

The EM field is decomposed in the Floquet harmonics:

$$\Phi_{pq}^{TE}(\vec{r}) = \frac{1}{\sqrt{d_x d_y}} \left(\frac{v_{pq}}{t_{pq}} \hat{x}_0 - \frac{u_{pq}}{t_{pq}} \hat{y}_0 \right) \Psi_{pq}(\vec{r})$$

$$\Phi_{pq}^{TM}(\vec{r}) = \frac{1}{\sqrt{d_x d_y}} \left(\frac{u_{pq}}{t_{pq}} \hat{x}_0 + \frac{v_{pq}}{t_{pq}} \hat{y}_0 \right) \Psi_{pq}(\vec{r})$$

with:

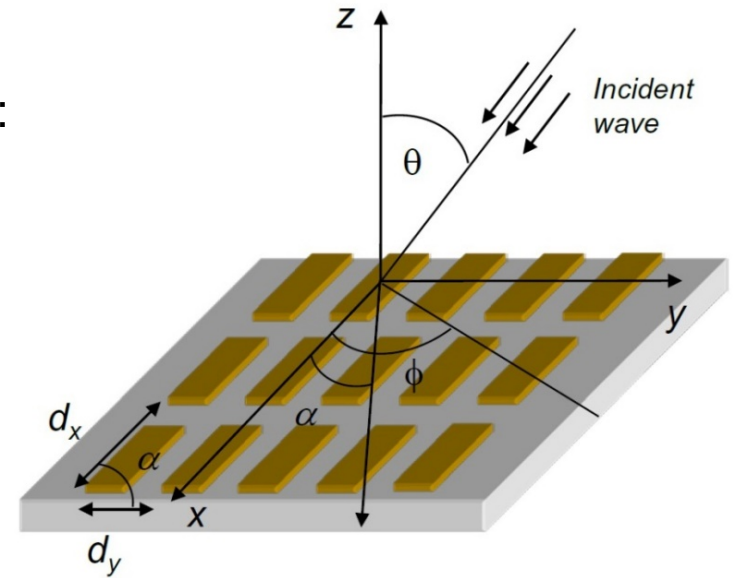
$$\Psi_{pq}(\vec{r}) = e^{i(u_{pq}x + v_{pq}y + \gamma_{pq}z)}$$

$$\begin{cases} \gamma_{pq} = \sqrt{k_0^2 - t_{pq}^2} & \text{for } t_{pq}^2 < k_0^2 \\ \gamma_{pq} = -i\sqrt{t_{pq}^2 - k_0^2} & \text{for } t_{pq}^2 > k_0^2 \end{cases}$$

$$u_{pq} = k_0 \sin \theta \cos \varphi + \frac{2\pi p}{d_x}$$

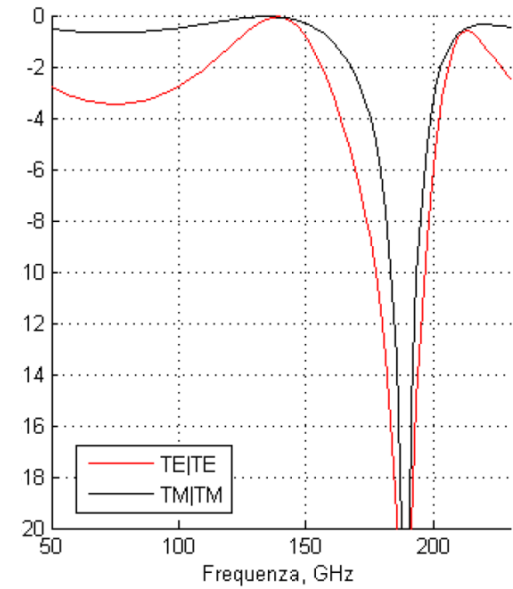
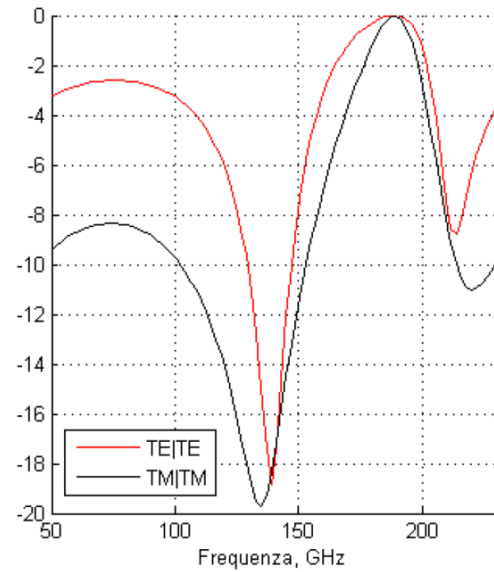
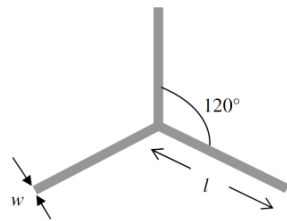
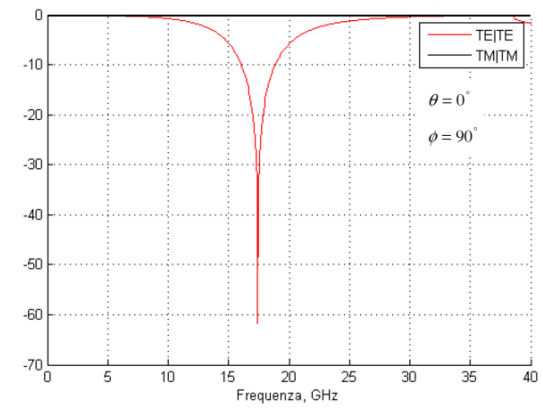
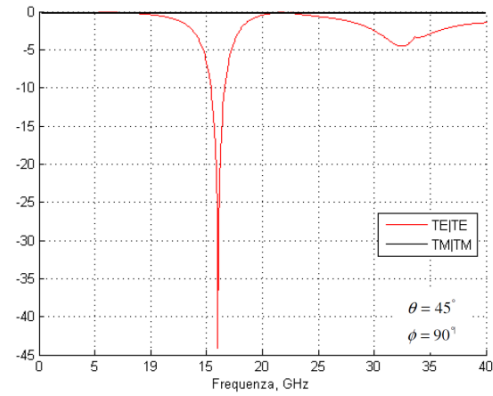
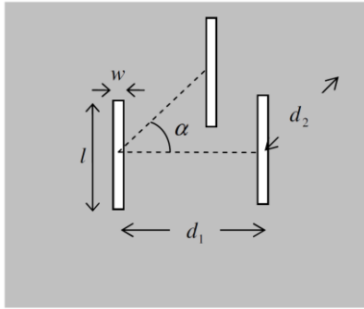
$$v_{pq} = k_0 \sin \theta \sin \varphi + \frac{2\pi q}{d_y} - \frac{2\pi p}{d_x \tan \alpha}$$

$$t_{pq}^2 = u_{pq}^2 + v_{pq}^2$$

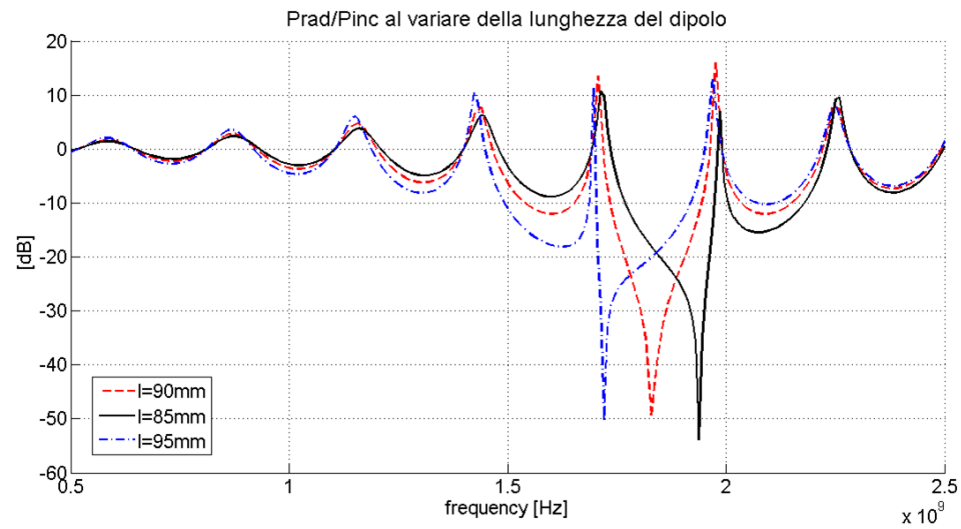
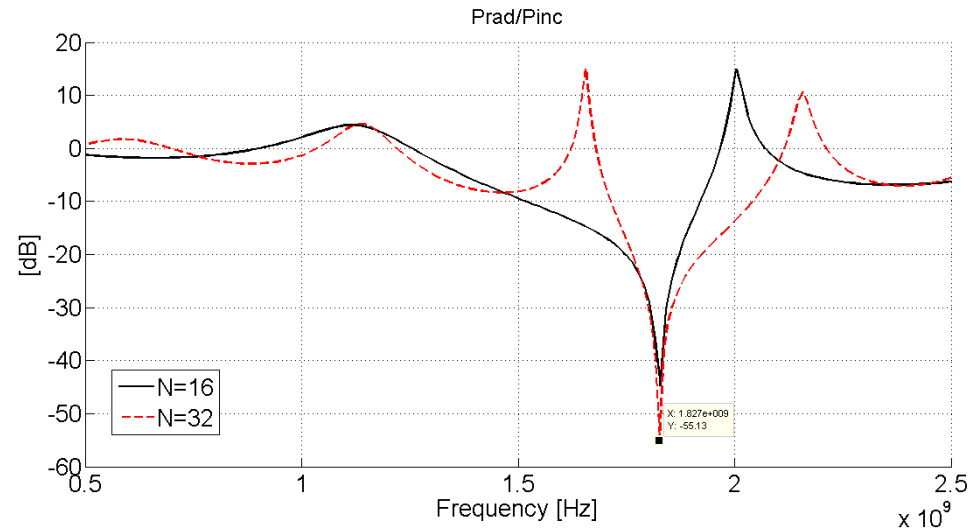
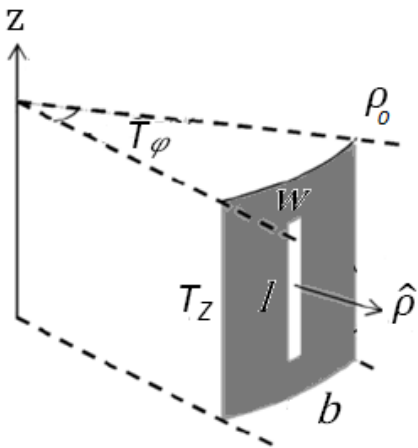
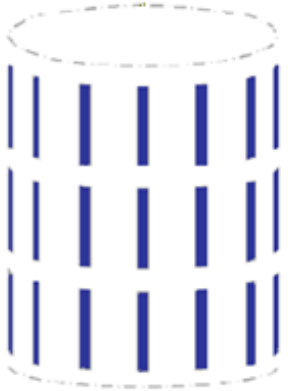


Metamaterials

FSS (2)

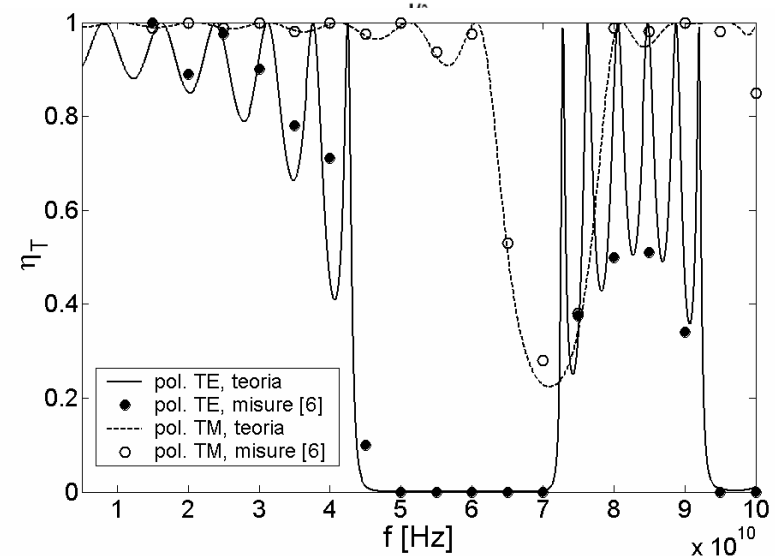
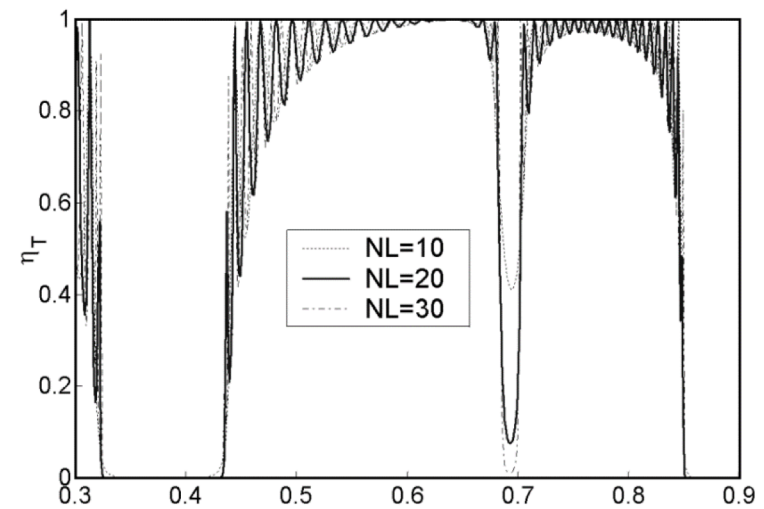
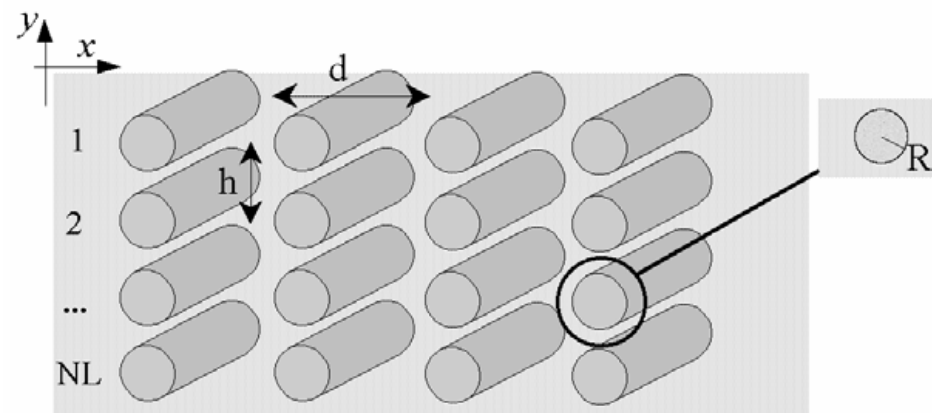
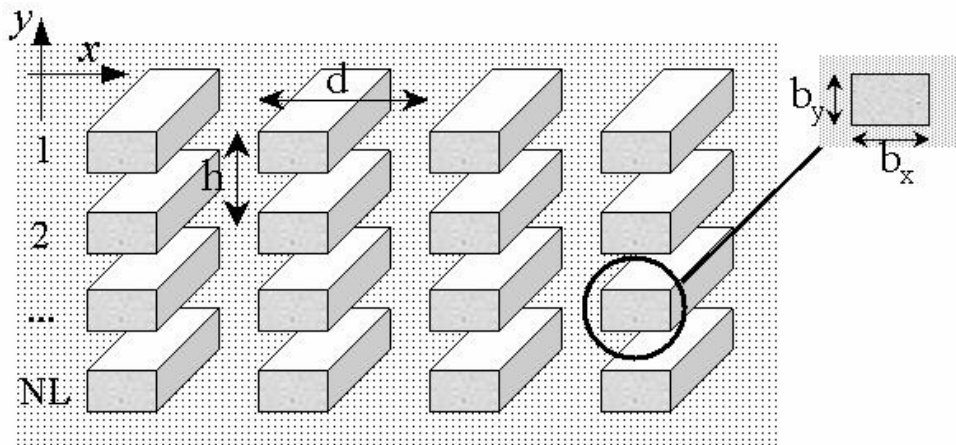


Metamaterials Cylindrical FSS



Metamaterials

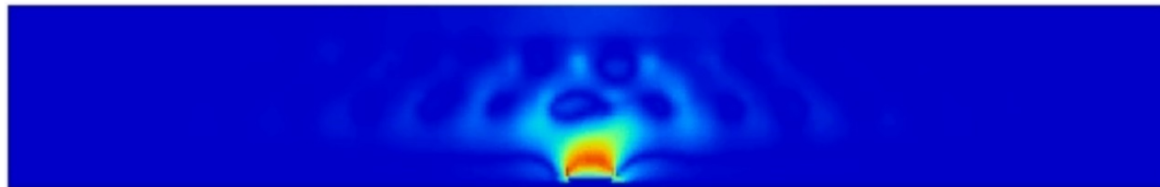
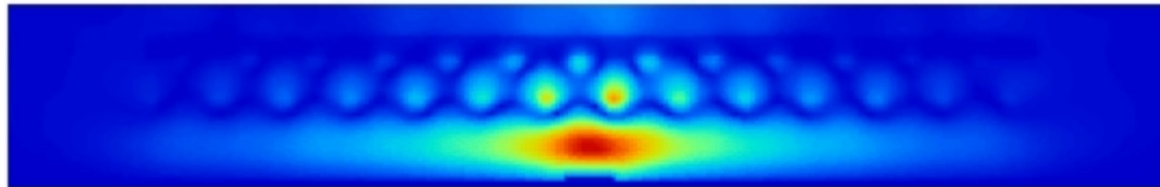
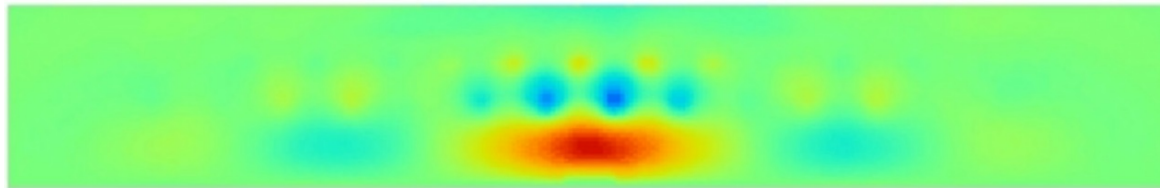
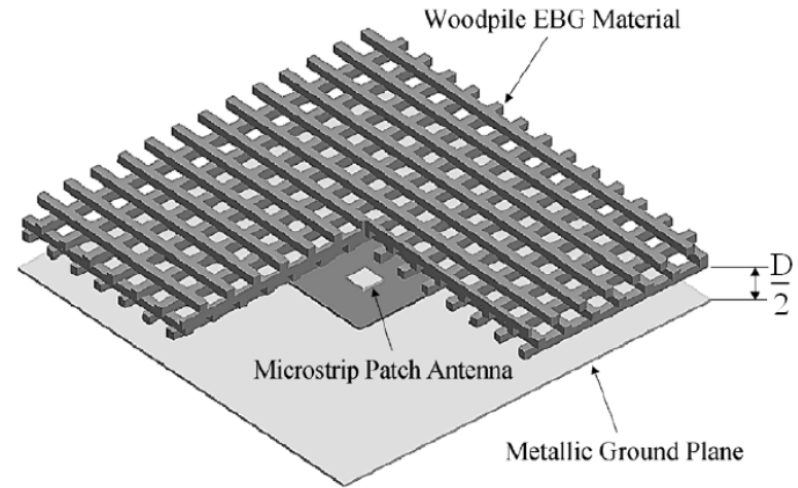
EBG (1)



Metamaterials

EBG (2)

FDTD method to simulate EBG applications.



Ex(t)

Pz(f)

0.44 V/m



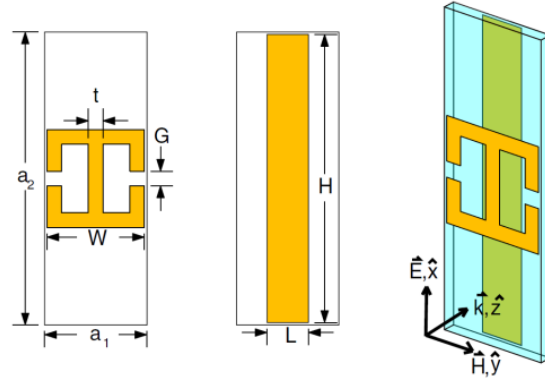
-0.44 V/m

Metamaterials Absorbers

$$t = 0.65 \text{ mm}$$

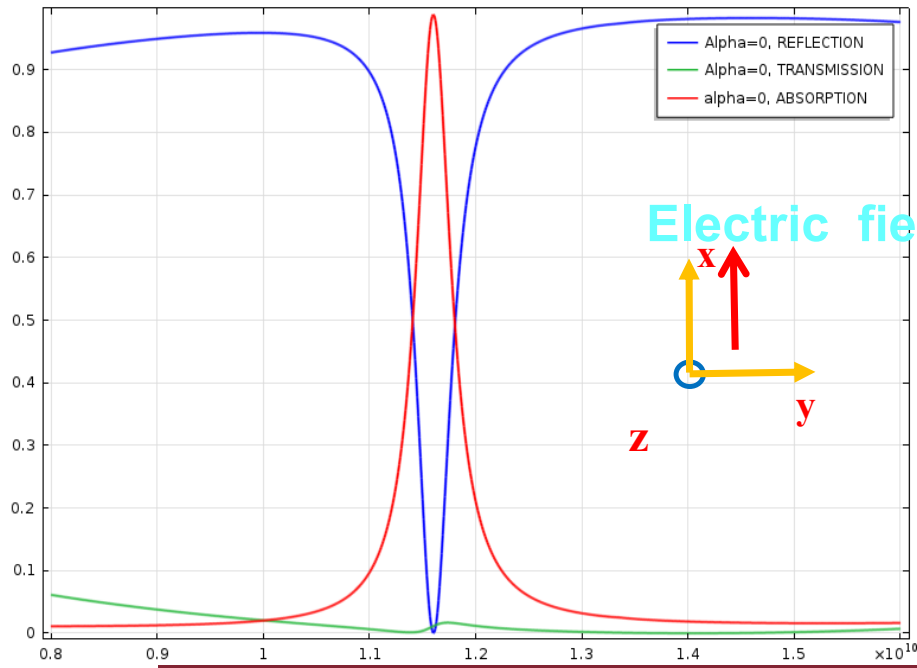
$$f = 11.6 \text{ GHz}$$

$$t / \lambda \sim 1/40$$

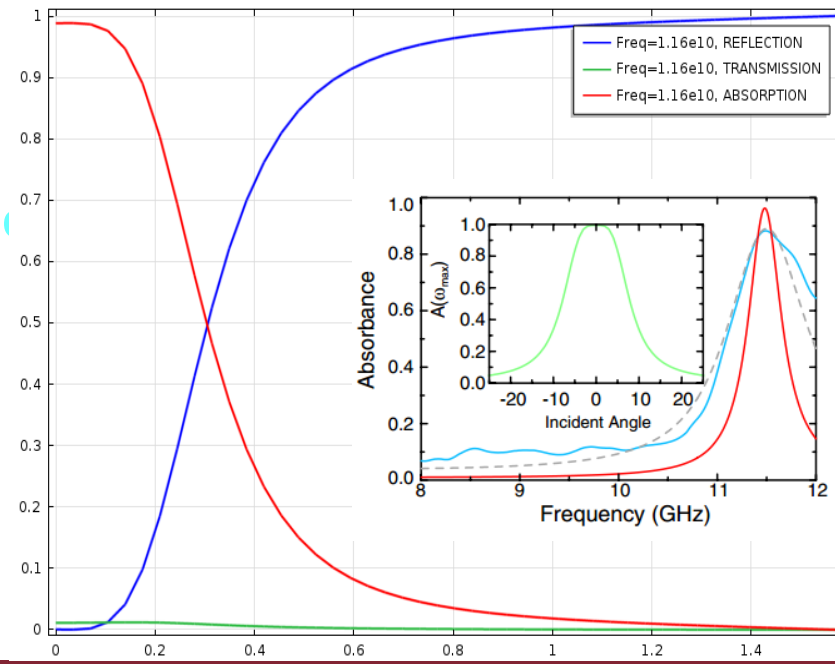


→ Biaxial

Frequency response (narrow)



Angular response (narrow)



Metamaterials

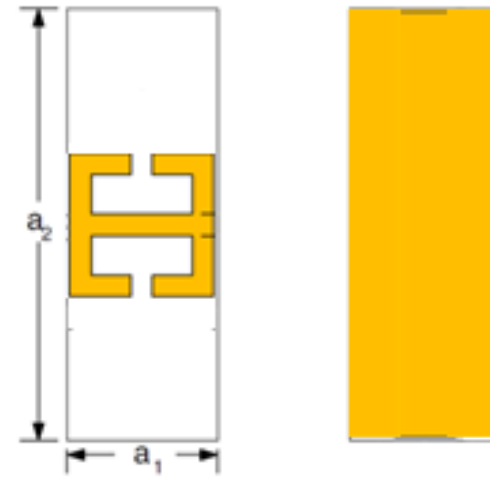
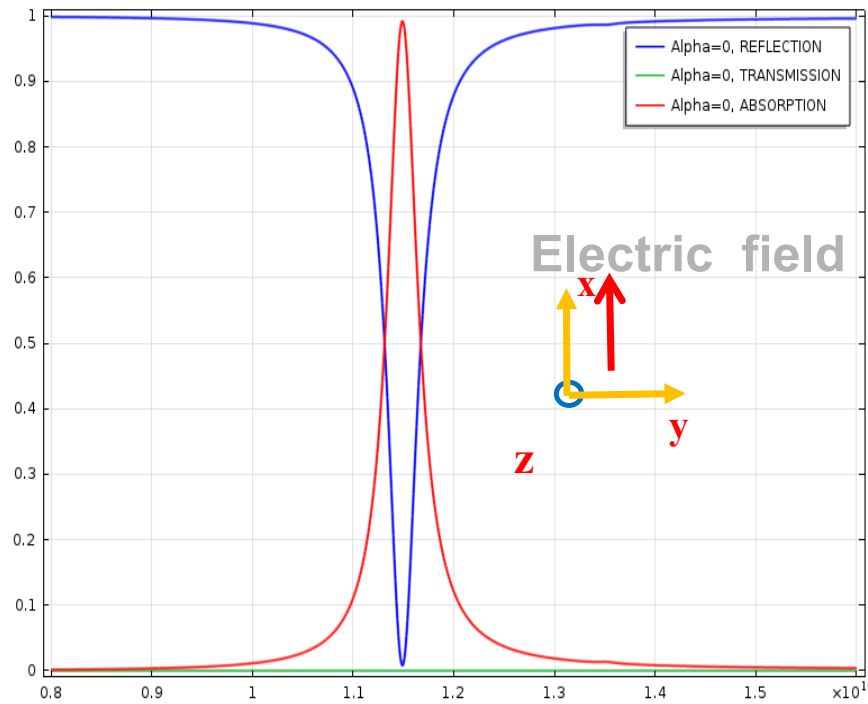
Absorbers: wide angular response (1)

$$t = 0.52 \text{ mm}$$

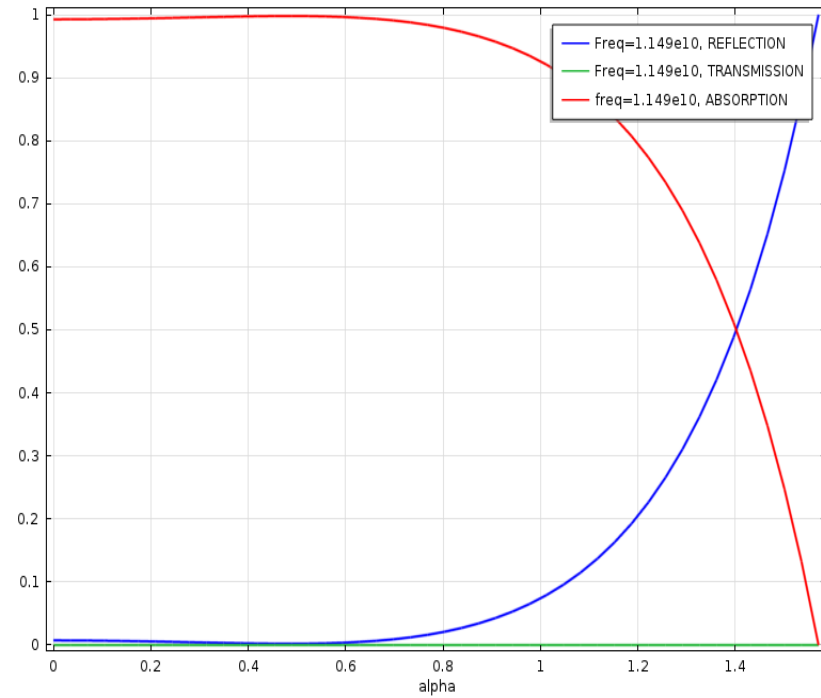
$$f = 11.6 \text{ GHz}$$

$$t / \lambda \sim 1/50$$

Frequency response (narrow)



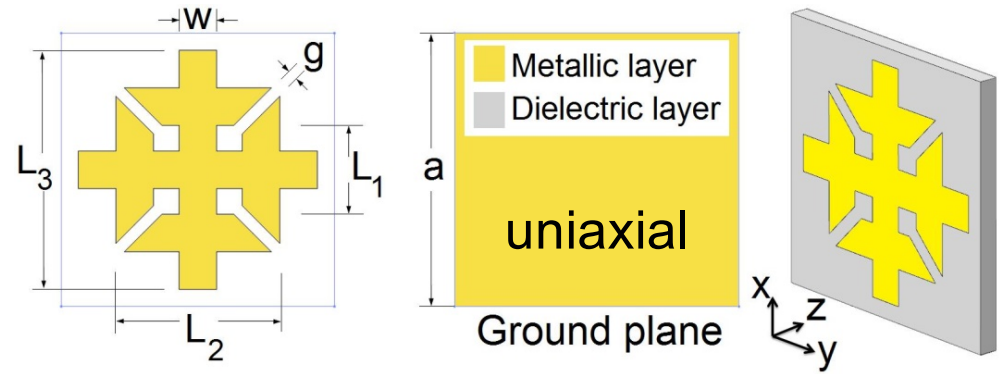
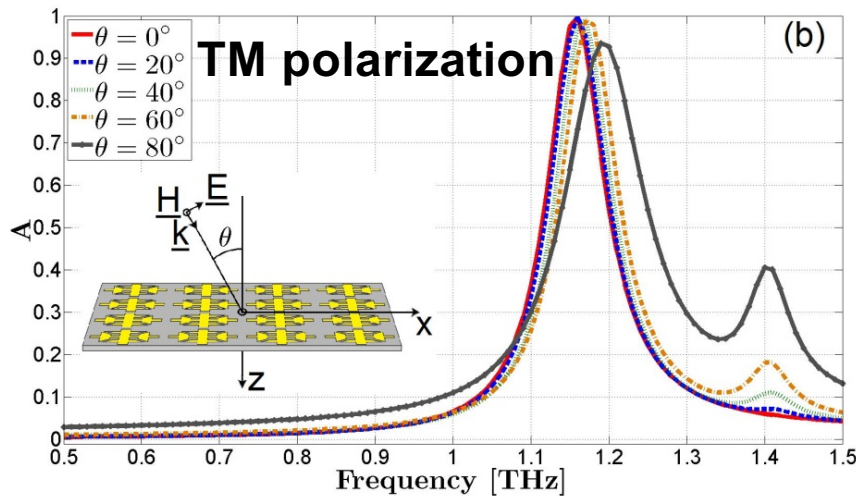
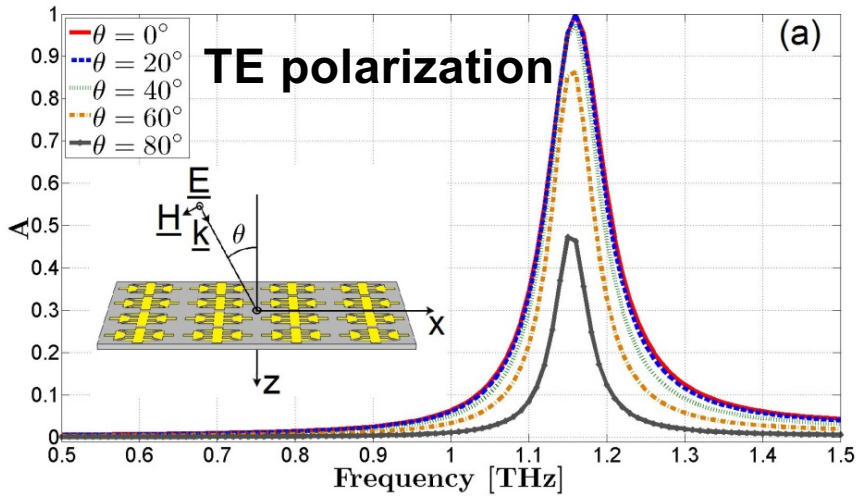
Angular response (wide)



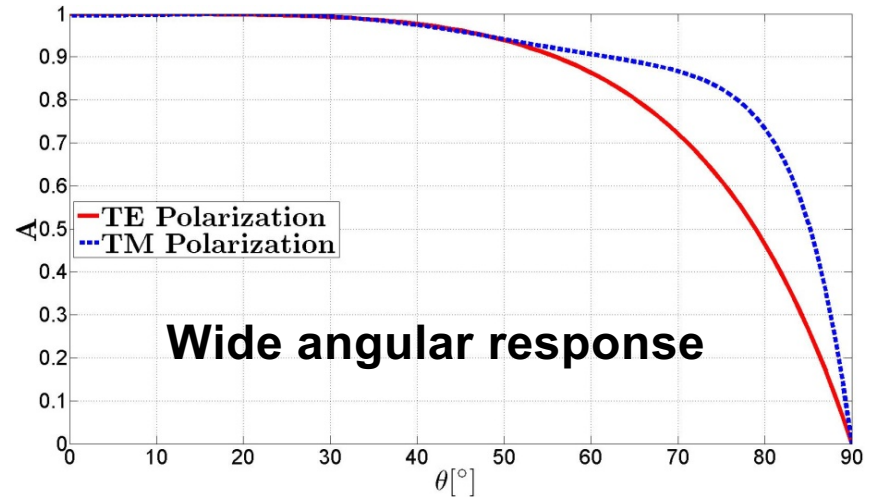
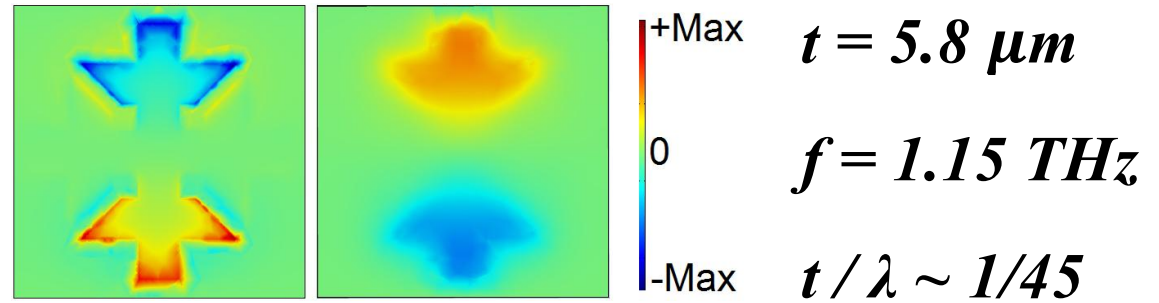
Metamaterials

Absorbers: wide angular response (2)

Narrow frequency response



Distributions of the z component electric field [V/m]

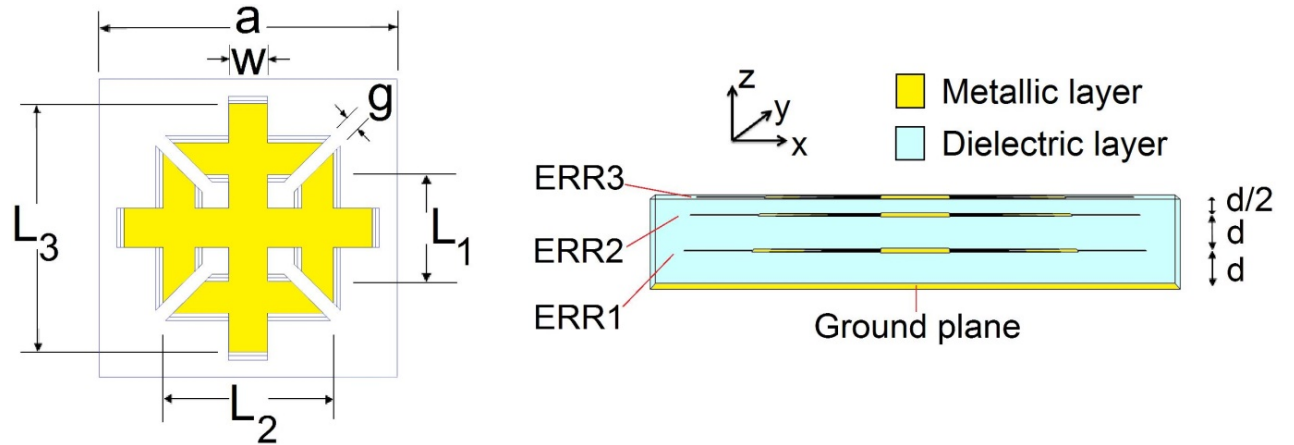
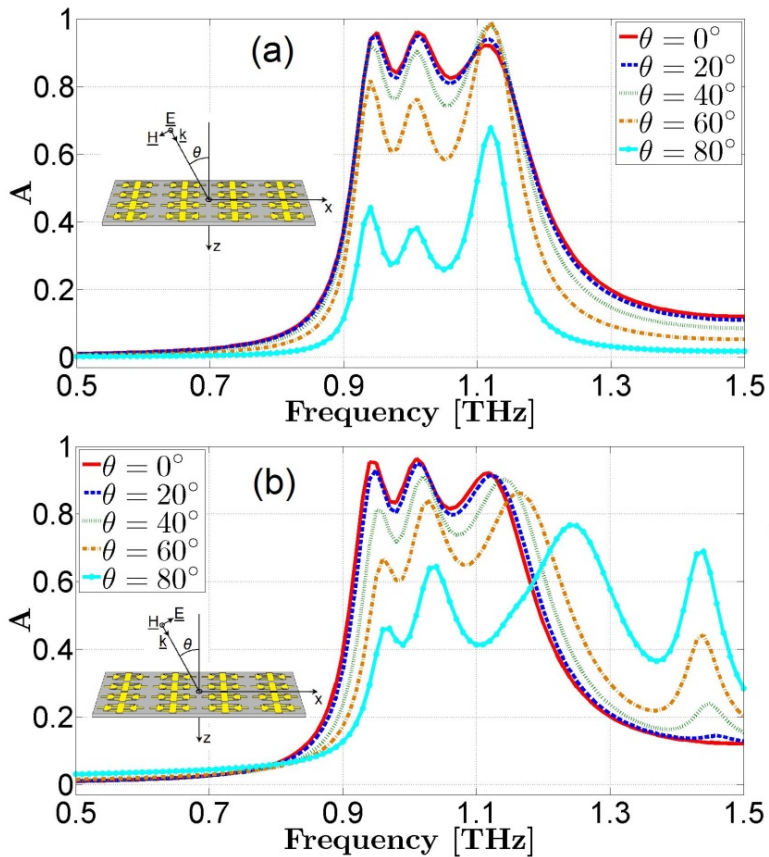


Metamaterials Broadband Absorbers

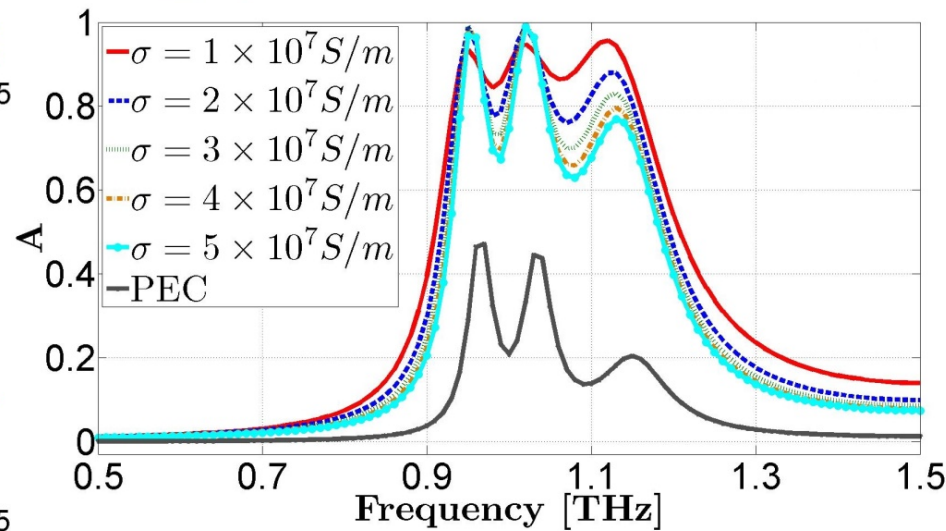
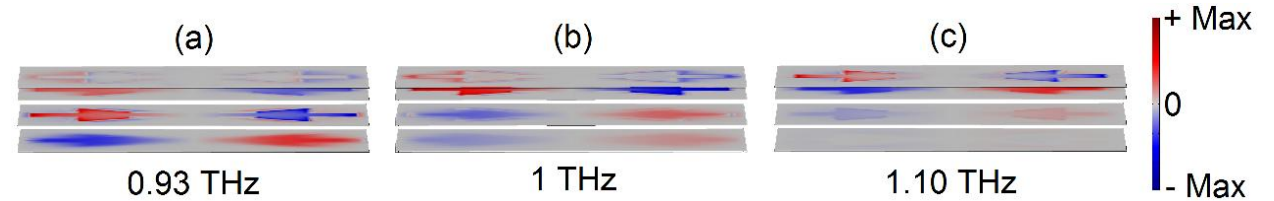
Wide frequency response:

(a) TE polarization

(b) TM polarization



Distributions of the z component electric field [V/m]



$$t = 14.5 \mu m$$

$$f = 1 THz$$

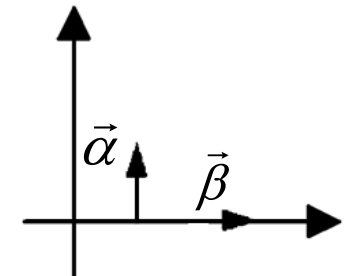
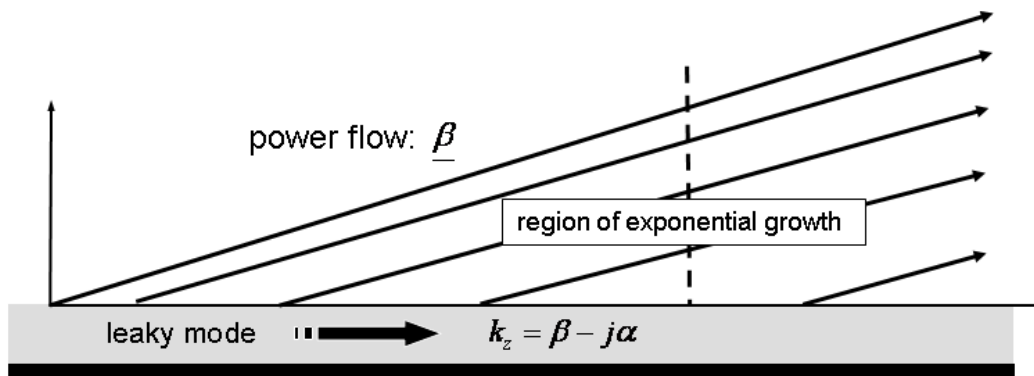
$$t / \lambda \sim 1/19$$

Leaky-Wave Antennas

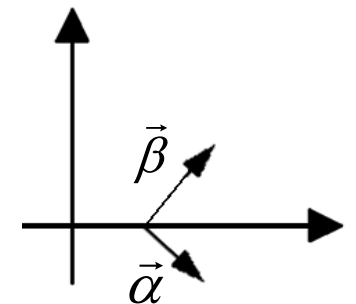
The electric field of a plane wave $\vec{E} = \vec{E}_0 e^{i\vec{k}\cdot\vec{r}}$, with: $\vec{k} = \vec{\beta} + i\vec{\alpha}$

In a lossless medium holds:
$$\begin{cases} \vec{\alpha} = 0 & \text{(homogeneous waves)} \\ \vec{\beta} \cdot \vec{\alpha} = 0 & \text{(inhomogeneous waves)} \end{cases}$$

In open waveguides, Leaky modes are related to radiation losses.



surface wave (proper)

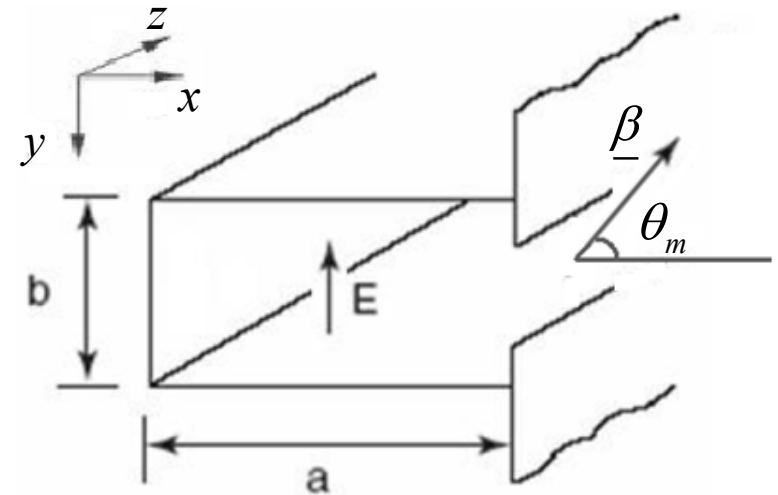


leaky wave (improper)

Leaky-Wave Antennas

The direction of $\vec{\beta}$ varies with frequency:

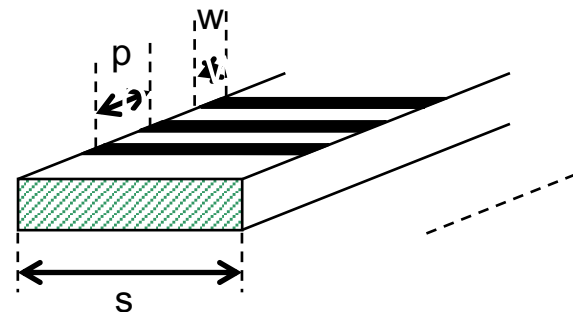
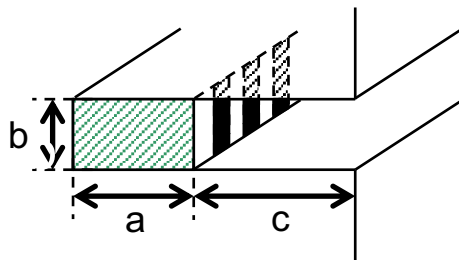
$$\sin \theta_m \cong \beta_z / k_0 \quad \Delta \theta \propto \frac{\alpha}{k_0}$$



It is possible to obtain a **frequency scanning** of the angle θ_m

The radiated beam has a narrow shape in the elevation (z, x) plane, and a broad shape in the cross (azimuth) plane (x, y).

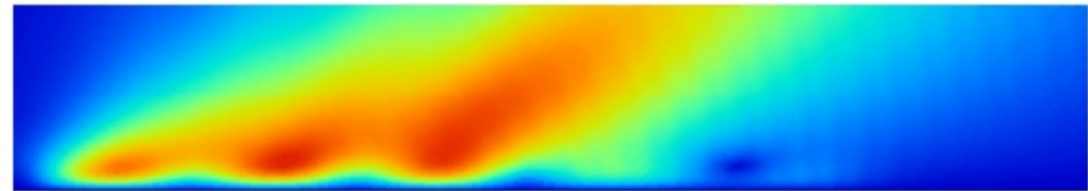
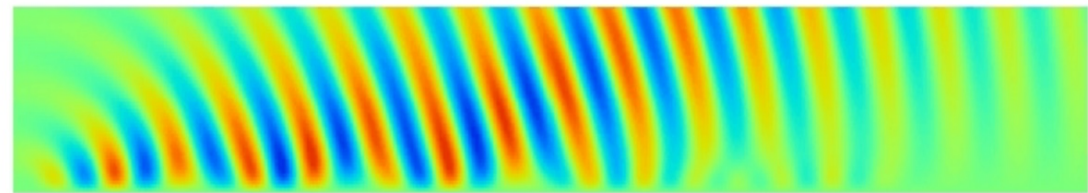
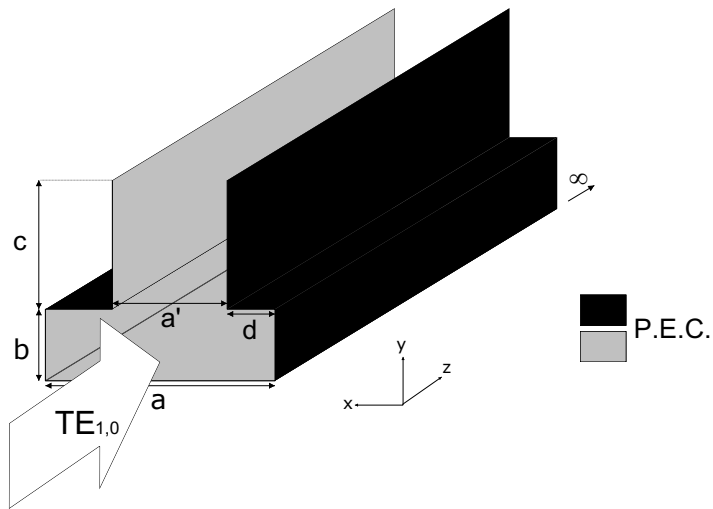
A pencil beam can be created by using a **phased array of line sources**.



Leaky-Wave Antennas

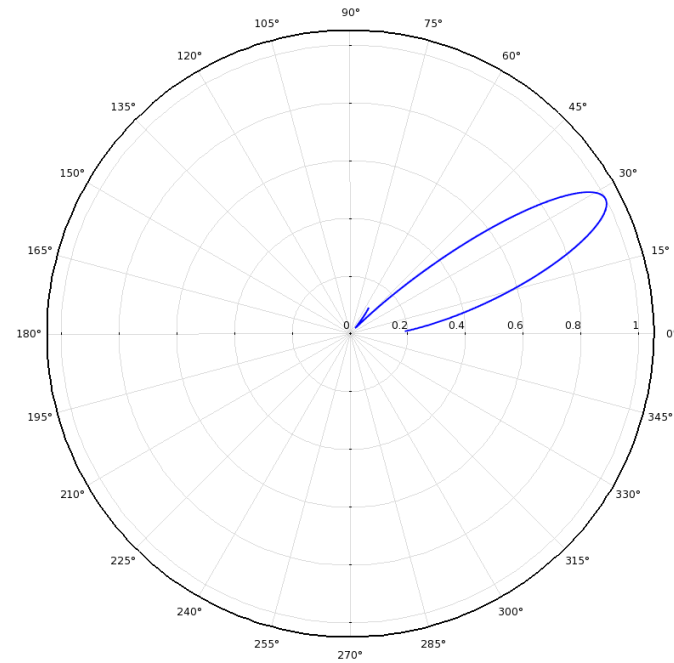
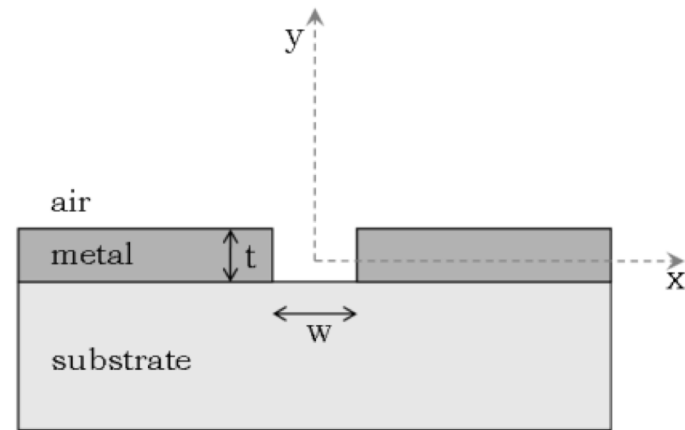
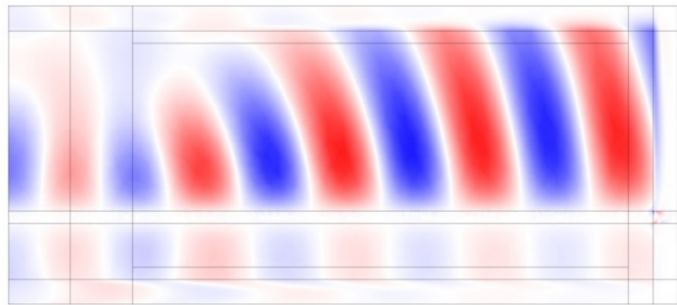
Microwave frequencies

FDTD method applied to study Leaky-Wave Antennas



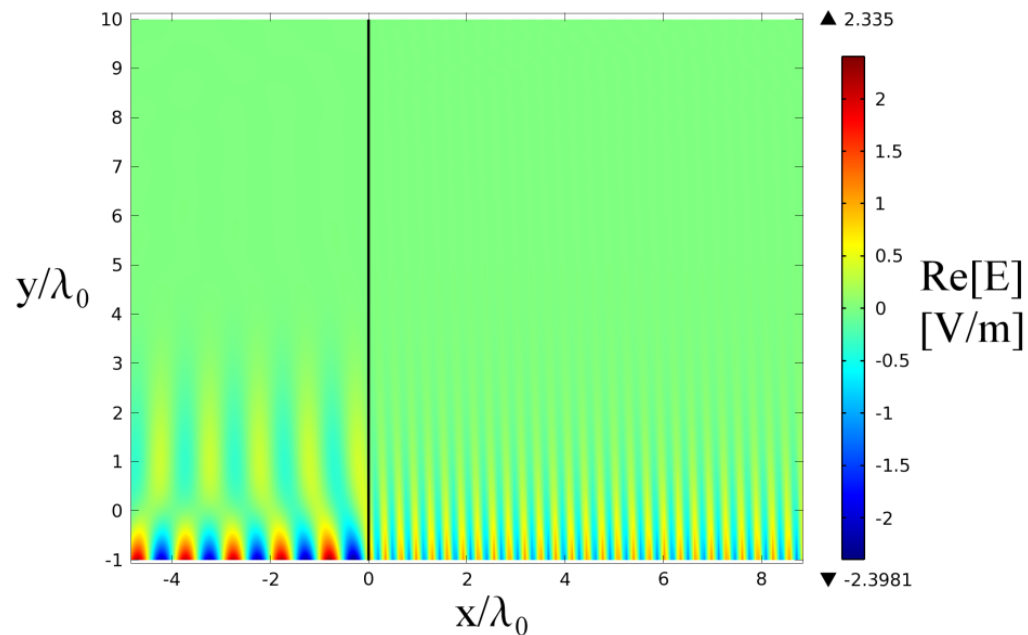
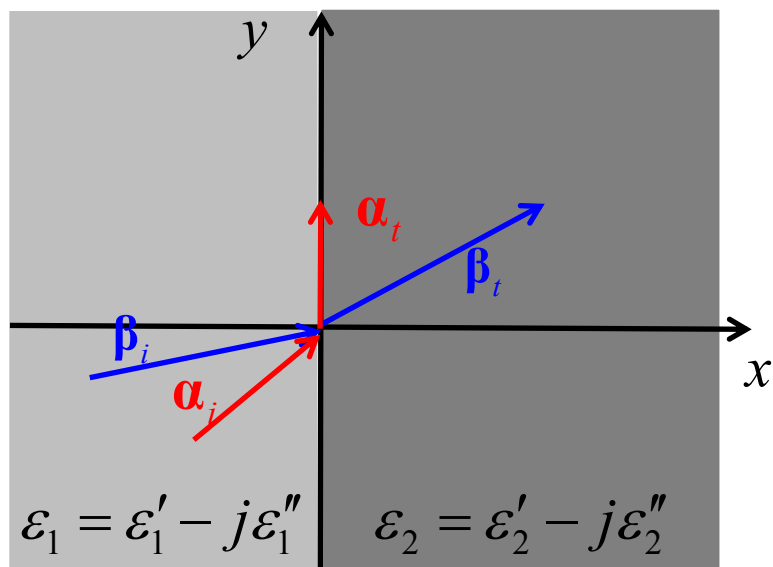
Leaky-Wave Antennas

Optical frequencies

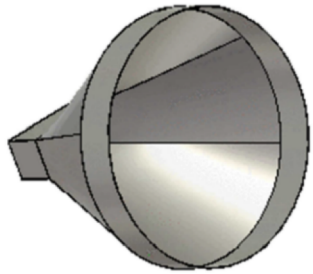


Deep Penetrating Waves

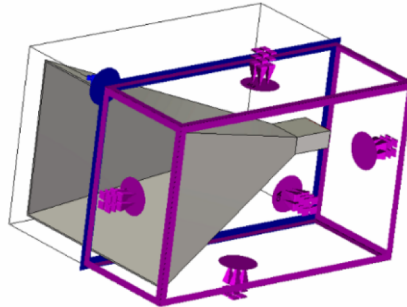
Inhomogeneous waves, under suitable conditions, are able to deeply penetrate in dissipative materials



Deep-penetration results (1)



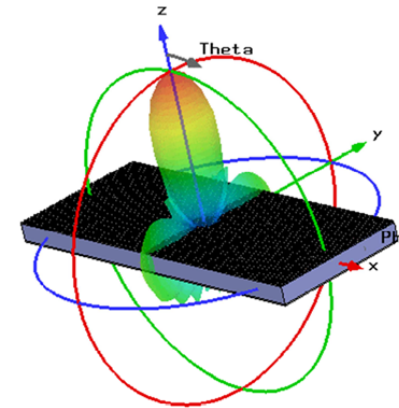
Circular Horn Antenna



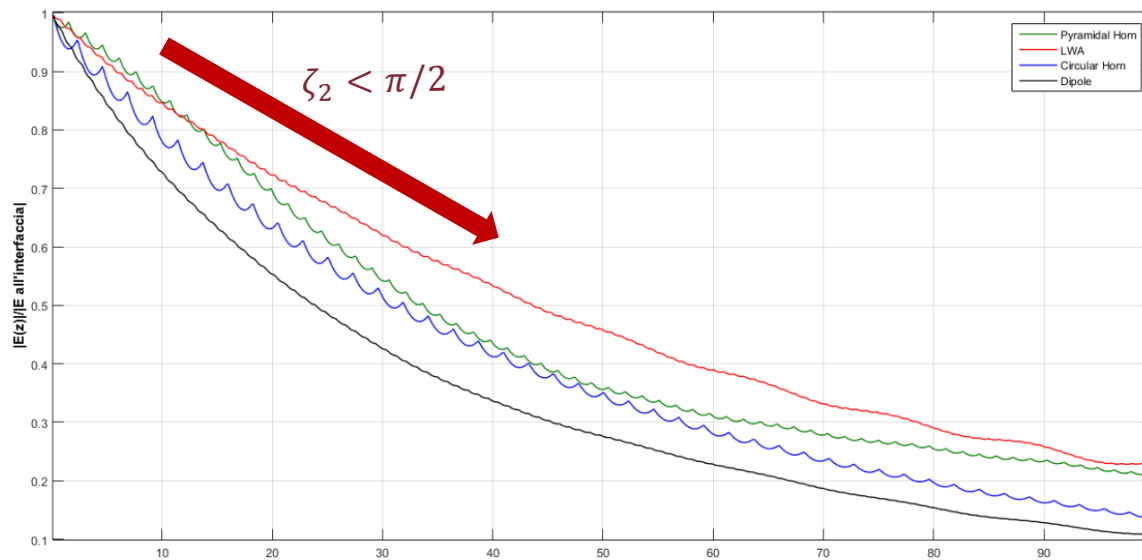
Pyramidal Horn Antenna



$\lambda/2$ dipole

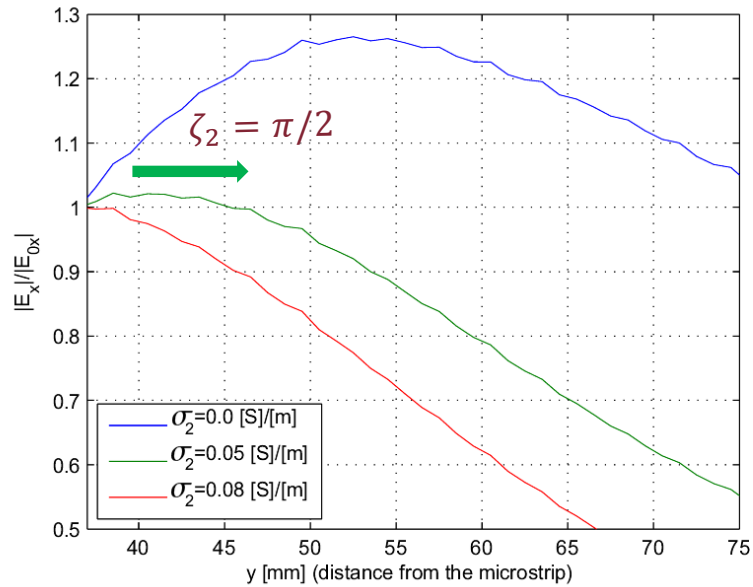


2D - LWA

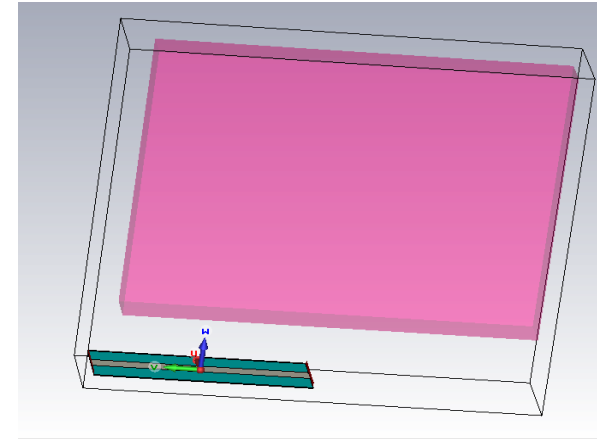


The maximum penetration is obtained with the LWA even though the attenuation vector is not parallel to the separation surface.

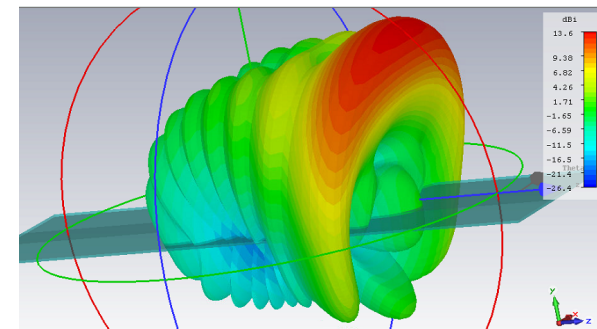
Deep-penetration results (2)



The uniform antenna produces an attenuation vector parallel to the separation surface when $\sigma = 0.05$ S/m

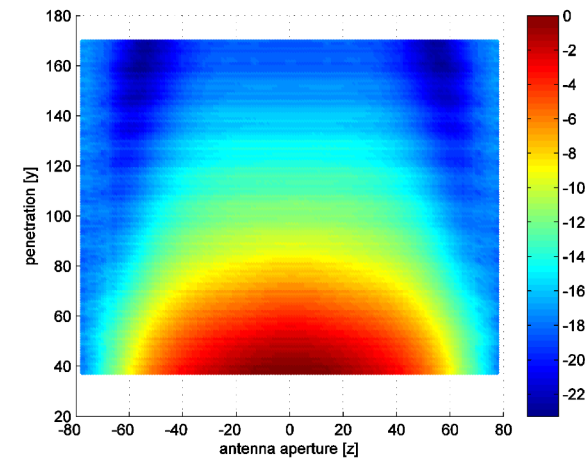
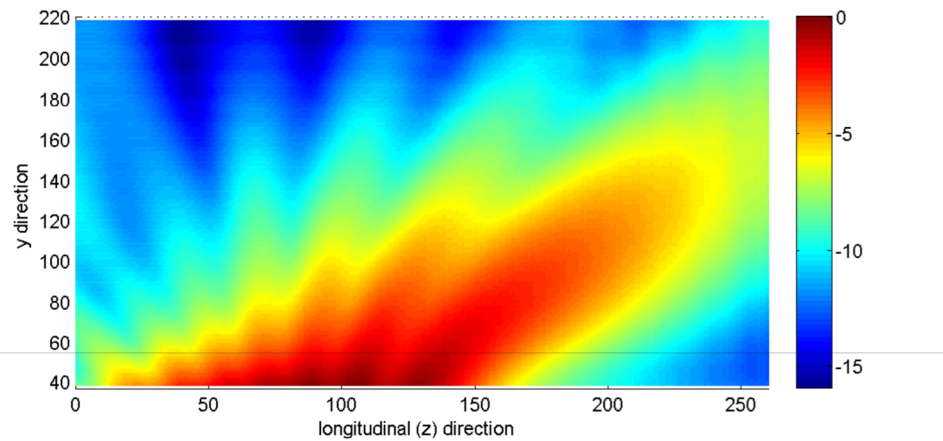


Antenna simulation setup with lossy Medium.



Deep-penetration results (3)

The result presented for the LWA can be compared with the penetration obtained with a conventional horn antenna (field normalised in respect to the maximum at the separation surface).

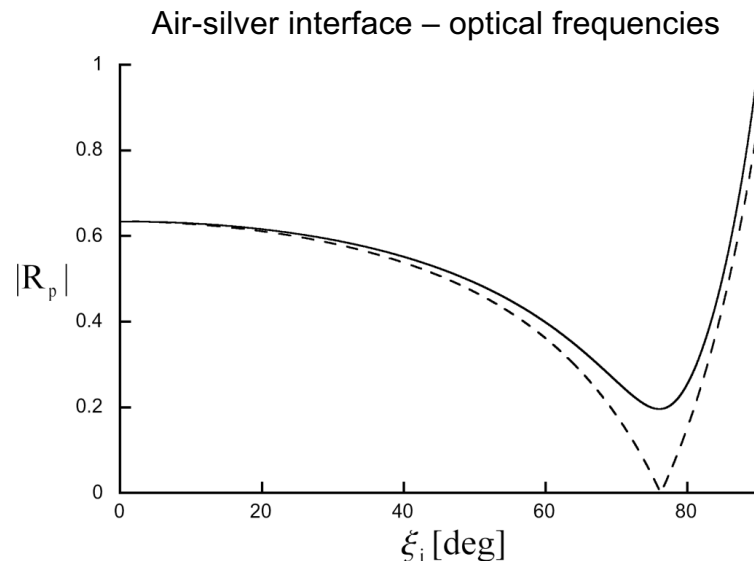


Normalised Magnitude of the electric field $|E_x|$ for a microstrip LWA (left) and a rectangular horn antenna (right) computed in dB from the maximum E-Field at the separation surface.

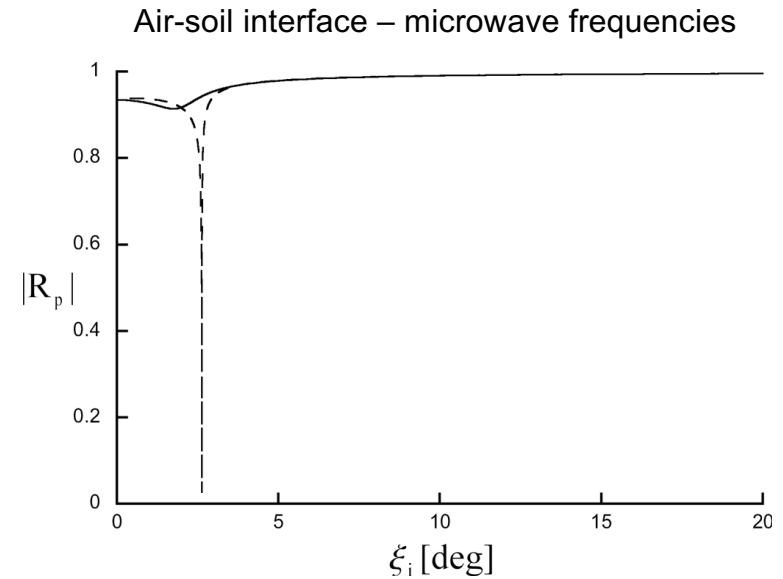
Total Transmission

It can be proved that inhomogeneous waves, differently from homogeneous ones, can be totally transmitted at an interface between a lossless and a dissipative material

Reflection coefficients



Solid line: homogeneous wave



Dashed line: inhomogeneous wave

FROM MAGNETIC RESONANCE IMAGING TO DIELECTRIC PROPERTIES EVALUATION OF A HUMAN TISSUE

Goal: non-invasive measurements of the electromagnetic properties of biological tissues in order to supply data to biomedical applications.

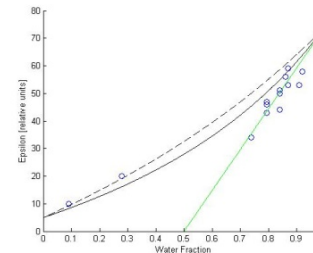
Process Framework:



```
(0008|0020) Study Date = 20010316
(0008|0021) Series Date = 20010316
(0008|0022) Acquisition Date = 20010316
(0008|0023) Content Date = 20010323
(0008|0030) Study Time = 143008
(0008|0031) Series Time = 143414
(0008|0032) Acquisition Time = 143415
(0008|0033) Content Time = 143013
(0008|0040) Accession Number =
(0008|0040) Modality = MR
(0008|0070) Manufacturer = GE Medical Systems
(0008|0080) Institution Name =
(0008|0090) Referring Physician's Name =
(0008|1010) Station Name = MRS1
(0008|1030) Study Description = BRAIN
(0008|1036) Series Description = ESE PD AXIAL OBL
(0008|1050) Performing Physician's Name =
(0008|1070) Operator's Name = EC
(0008|1090) Manufacturer's Model Name = SIGNA
(0010|0010) Patient's Name =
(0010|0020) Patient ID = 123565
(0010|0030) Patient's Birth Date =
(0010|0040) Patient's Sex = M
(0010|1010) Patient's Age = 028Y
(0010|1030) Patient's Weight = 61.25kg
```

$$\frac{1}{wf} = A + \frac{B}{T1}$$

$$Wf = \frac{S0(tissue)}{S0(ref)}$$



- custom models
- computer simulations for thermal-ablation therapy

in collaboration with prof. Marta Cavagnaro (“La Sapienza” University) and ENEA-Casaccia Research Center

FROM MRI TO DIELECTRIC PROPERTIES EVALUATION



MRI Basic and Sequences:

- Relaxation parameters and constants;
- Gradient Echo and Spin Echo properties;
- MRI Acquisitions:
 - Dept. of Radiological Sciences, etc.,
 - “La Sapienza” University



DICOM Import:

- MatLab script and procedures development;
- SW program development using ITK (open source library) on linux platform.

Dielectric Properties from Water %:

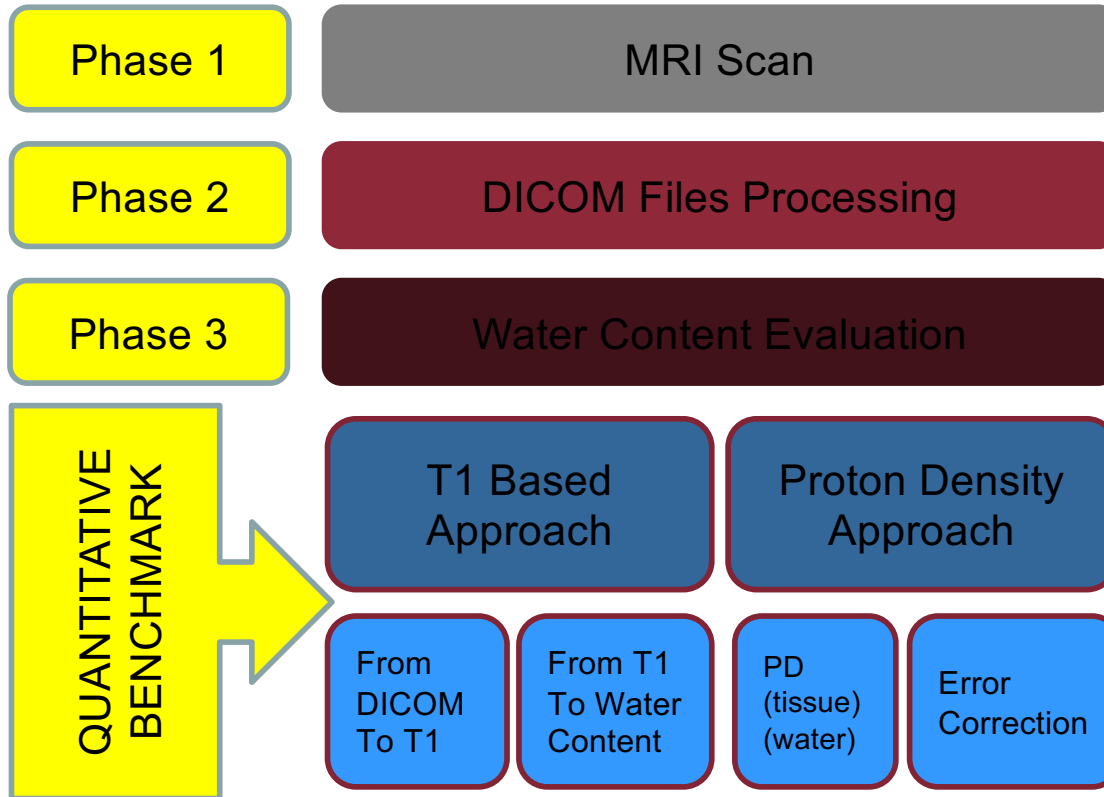
- Literature survey: tissues water content;
- Main available models benchmark;
- Development (ongoing) of a parametric model based on Debye equations and info about tissues composition collected during survey;
- Benchmarking (ongoing) between models and measurements.

Water Content Evaluation from Voxels:

- Analysis, replicas and benchmarking;
- MatLab script development;
- Validation on “ad hoc” pre-built phantoms.



Process overview (first 3 phases)



T1 based Approach

- T1 evaluation:** performing a ratio between the corresponding raw data (signal intensity) of two acquisitions for the same slice with different TR (where TR1 must be shorter than TR2) .

$$\frac{S1}{S2} = K \frac{1 - 2e^{\frac{-TR1+TE}{2T1}} + e^{\frac{-TR1}{T1}}}{1 - 2e^{\frac{-TR2+TE}{2T1}} + e^{\frac{-TR2}{T1}}}$$

- Water fraction from T1:**

$$\frac{1}{wf} = A + \frac{B}{T1}$$

Magnetic Field Strength	A	B (ms)
0.5 Tesla	0.948	227
1.0 Tesla	0.935	283
1.5 Tesla	0.921	341

WSN and/or Remote Sensing for monitoring of a scenario

WSN – Smart Objects

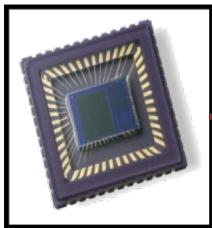
Each node includes:

- one or more sensors
- a microcontroller
- a power source
- a communication device.

Level and pressure detectors with energy harvesting



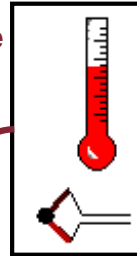
Image sensor for target detection



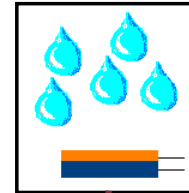
GPS navigation data



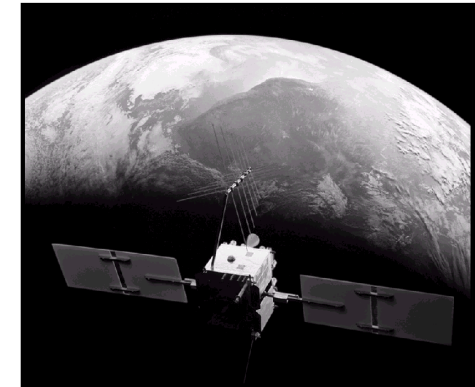
Temperature Sensor



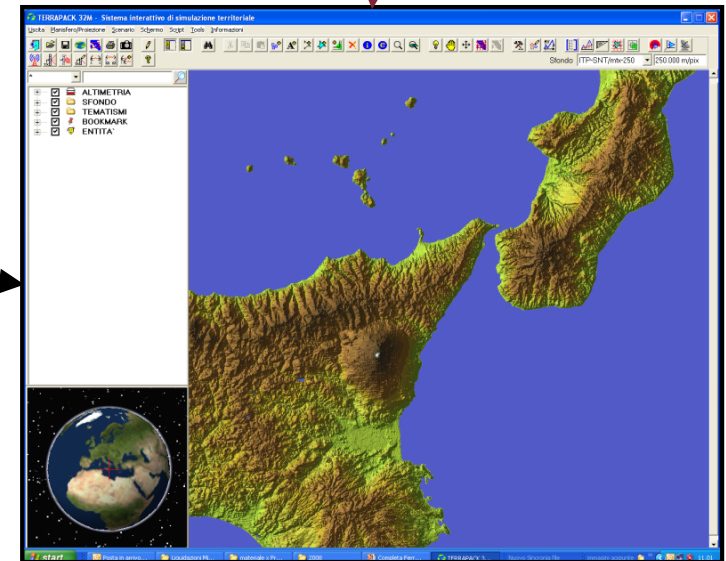
Moisture Sensor



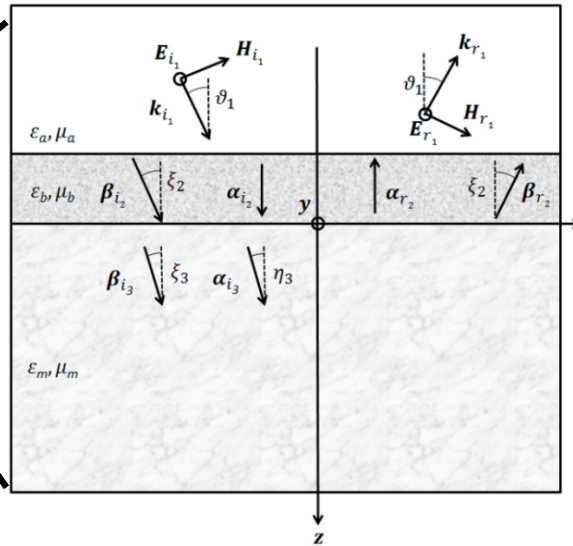
Remote sensing



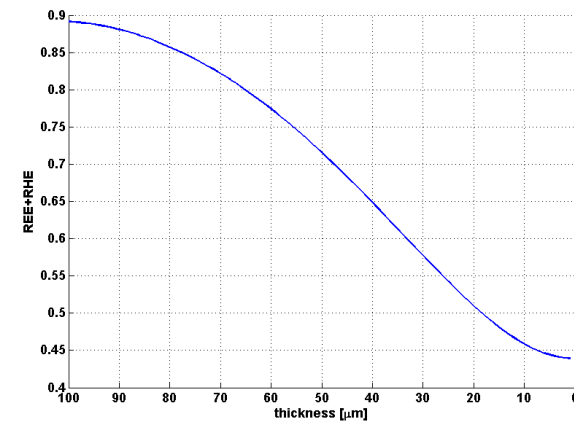
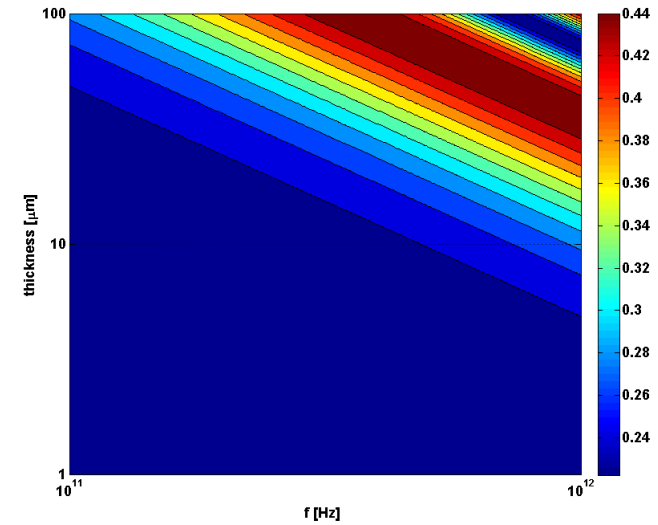
Microcontroller PIC and Transceiver



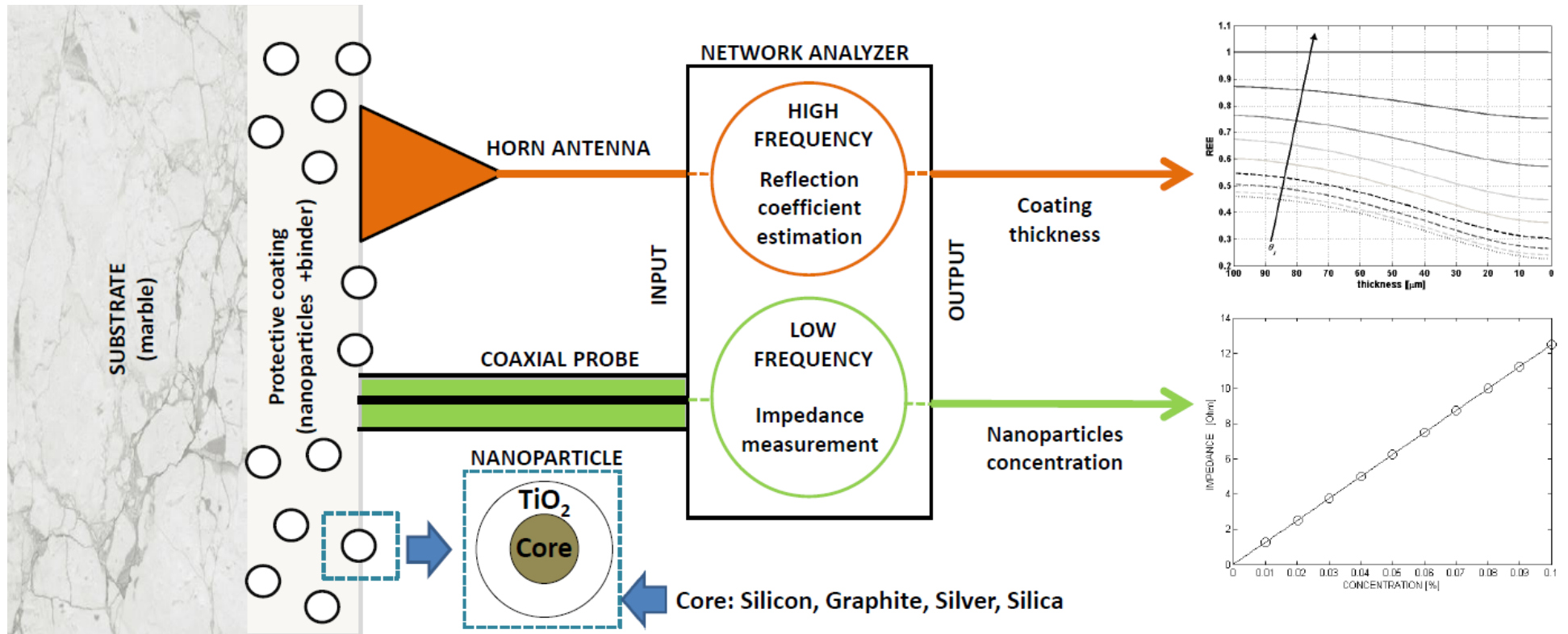
Cultural Heritage Applications



Geometric and structural characterization by electromagnetic excitation on marble objects of historical and artistic interest



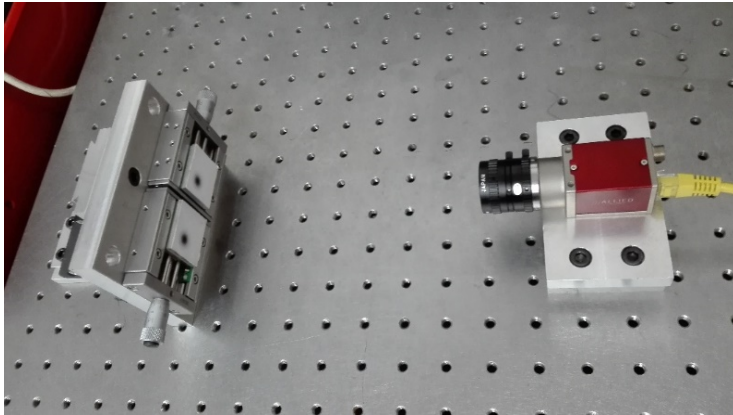
Cultural Heritage Applications



Schematic representation of the monitoring system of the protective coating. The high frequency excitation is used for the estimation of the coating thickness, while the low frequency excitation is used for the estimation of the nanoparticles concentration.

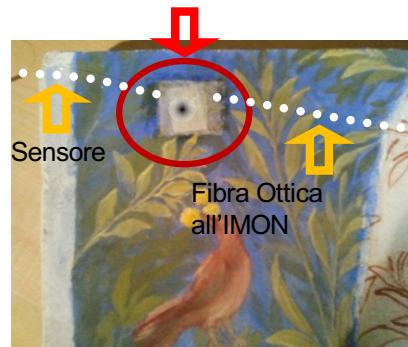
Cultural Heritage Applications

Tag Recognition: a new methodology for the structural monitoring of cultural heritage

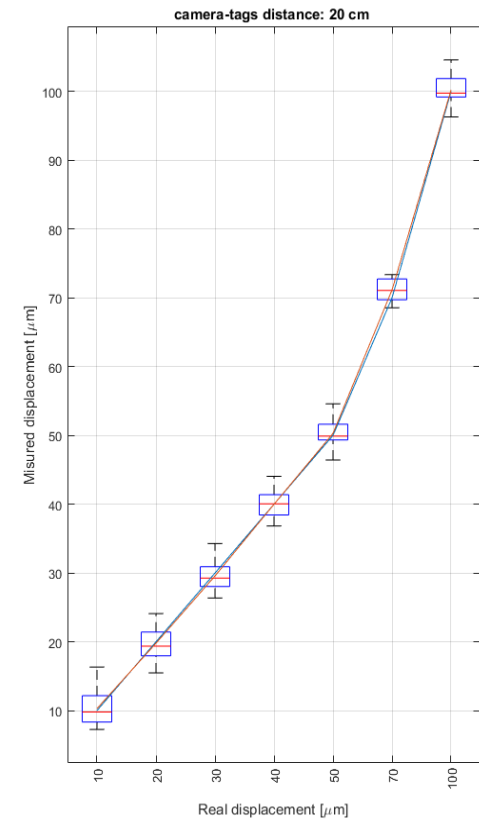


Test Bench in controlled environment

The minimum invasiveness of this methodology permits to preserve the aesthetic appearance, a fundamental requirement of cultural heritage. The core of the acquisition system is composed by two small adhesive tags to be attached on the artwork surface, and a high-resolution camera acquiring images of the tags. The relative distance between the optical tags is determined using advanced least-squares fitting of quadratic curves algorithms for the objective function.



System test on a fresco

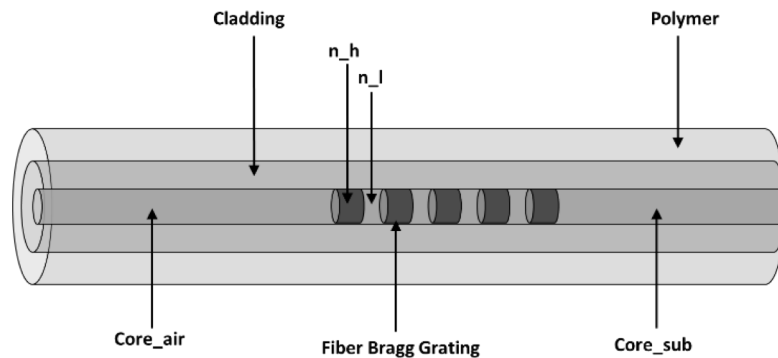


Relative displacement between the optical tags. The camera-tags distance is 20 cm

Cultural Heritage Applications

FBG Multifunctional pH Sensor - Monitoring the Rain in Cultural Heritage

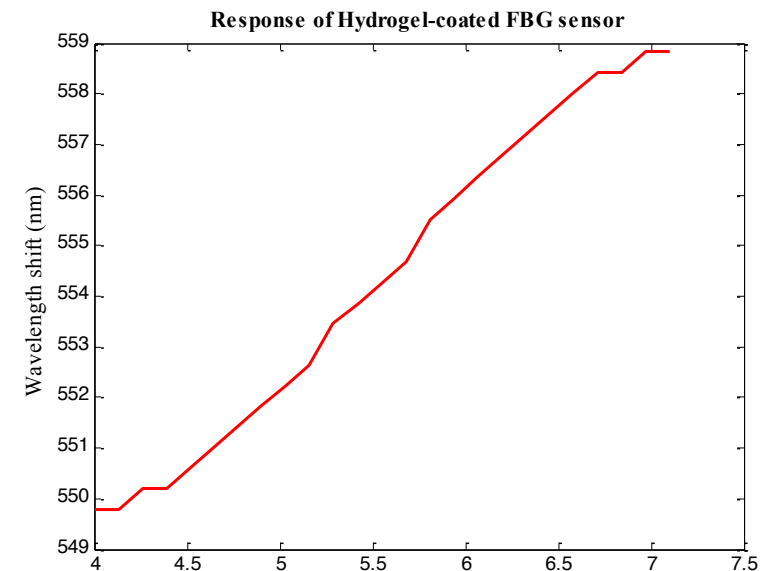
The FBG Multifunctional pH sensor is an innovative new fiber optic sensor that combines Fiber Bragg Gratings (FBG) coated with pH responsive polymers for monitoring the pH of the rains on critical and prestigious monuments is proposed. Monitoring the pH of the water can be used by experts to predict and control the corrosion phenomenon of specific materials, especially limestone and marble, and thus scheduling the timely restoration.



Schematic drawing of polymer-coated FBG pH sensor.



Neptune Fountain by Giambologna – Bologna, Italy.



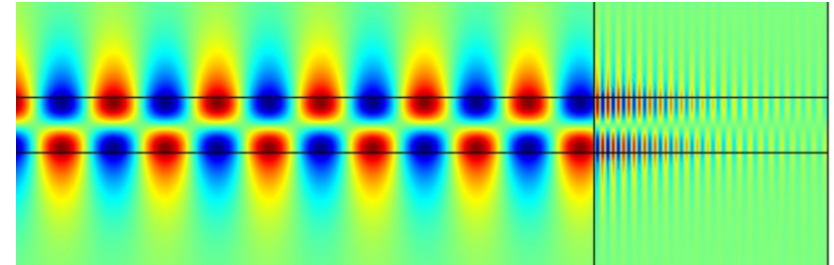
Response of a Fiber Bragg Grating coated with Hydrogel as a function of pH.

Principal collaborations

Department of Engineering
(at Roma Tre University)



Department of Radio Science and Engineering
(at Aalto University, Finland)



Humanitarian Demining Laboratory
(at “La Sapienza” University)

